Met Office

Describing the development of the new FOAM-NEMOVAR system in the global 1/4 degree configuration

Forecasting Research Technical Report No: 578

June 14, 2013

Jennifer Waters, Daniel Lea, Matthew Martin, David Storkey and James While

Abstract

A new incremental 3DVAR data assimilation scheme, NEMOVAR, has been implemented and tested in FOAM in the global ORCA025L75 configuration. This document provides a detailed description of the system and the developments made by the Met Office. These include some small changes to the balance relationships, implementation of sea ice concentration data assimilation and bias correction schemes for satellite sea surface temperature (SST) and height (SSH) data, developments to specification of the background error standard deviations, new paramerisations for the background error correlation lengthscales and a new, efficient technique for generating the normalisation factors for flow dependent vertical correlation lengthscales. The new system has been compared with the preceding FOAM analysis correction data assimilation system. The key results are that NEMOVAR provides significant improvements to surface fields with a 28% reduction in SST root mean square error (RMSE), a 20$\%$ reduction in sea ice concentration RMSE and a 3.5$\%$ reduction in SSH RMSE. The results for profiles are more mixed with an increase in salinity RMSE in the top 300m. There is an overall improvement to temperature profile RMSE but a degradation between 100m and 400m largely associated with an increased mean error in NEMOVAR. NEMOVAR was implemented operationally at the Met Office in 2012.

1 Introduction

The Met Office's Forecasting Ocean Assimilation Model (FOAM) has been run as a global operational system since 1997. The model produces analyses and forecasts of temperature, salinity, currents, sea surface height and sea ice. The products are used by the Royal Navy, commercially and for research purposes and contribute to the MyOcean project. Since 2008 the hydrodynamic model in FOAM has been the Nucleus for European Modelling of the Ocean (NEMO) model (Madec [2003]).

We have updated the data assimilation scheme in FOAM to the variational system, NEMOVAR (Mogensen [2009]). This replaced our current analysis correction data assimilation scheme (Martin et al. [2007]) in the operational system in 2012. This report describes the status of the developments to NEMOVAR at the Met Office as of July 2012 and presents results from a trial performed at that time. Some subsequent developments have been made to NEMOVAR and these are discussed in section 9.

NEMOVAR is an incremental 3DVAR-FGAT (first guess at appropriate time) data assimilation scheme for the dynamical ocean model in NEMO and is a collaboration between CERFACS, ECMWF, the Met Office and INRIA/LJK. A variational scheme has been chosen for the new operational system rather than an ensemble method mainly due to the limitations of an achievable ensemble size operationally at the Met Office. NEMOVAR has been specifically developed for NEMO and the collaboration ensures significant development of the scheme. Features implemented in NEMOVAR include multivariate balance relationships (Weaver et al. [2005]) and an implicit diffusion operator

© Crown Copyright 2013

correlation model (Mirouze and Weaver [2010]).

A detailed description of NEMOVAR is provided by Mogensen et al. [2012], so below we focus on the developments made at the Met Office, and other aspects relevant to the results. The results and developments discussed are for the global $\frac{1}{4}$ degree configuration. In sections 2-7 a description of the 3D var system, the multivariate balance relationships, the specification of the error covariances and the bias correction schemes are provided, with a particular focus on developments and tuning implemented at the Met Office. Throughout this report the FOAM configuration with NEMOVAR is referred to as FOAM-NEMOVAR, while the preceding operational configuration is referred to as FOAM-AC. As well as differences in the data assimilation schemes, there are also some differences in the model configuration, model physics and initial conditions in FOAM-NEMOVAR compared to FOAM-AC. These differences are described in detail in section 5. In section 7 the bias correction schemes implemented at the Met Office are discussed. Finally, in section 8 results from a FOAM-NEMOVAR re-analysis are presented and assessed compared to a FOAM-AC re-analysis. The main findings are discussed and plans for additional developments and improvements described.

2 Variational Data Assimilation

The 3D VAR incremental cost function is written as follows:

$$J(\delta\mathbf{x}) = \frac{1}{2}(\delta\mathbf{x})^T\mathbf{B}^{-1}(\delta\mathbf{x}) + \frac{1}{2}(\mathbf{d} - \mathbf{H}\delta\mathbf{x})^T\mathbf{R}^{-1}(\mathbf{d} - \mathbf{H}\delta\mathbf{x}) \quad (1)$$

where $\mathbf{x}$ is the ocean state vector, $\mathbf{x}_b$ is the background state, $\mathbf{y}$ are the observations, $\delta\mathbf{x} = \mathbf{x} - \mathbf{x}_b$ are the increments and $\mathbf{d} = \mathbf{y} - \mathbf{H}(\mathbf{x}_b)$ are the innovations. The ocean state vector contains temperature (T), salinity (S), sea surface height (η), horizontal velocities ($\mathbf{u}$) and sea ice concentration (C). The observation error covariance matrix is denoted by $\mathbf{R}$, the observations errors are generally assumed uncorrelated and therefore $\mathbf{R}$ is a diagnonal matrix. The background error covariance matrix, $\mathbf{B}$, is a large, full rank matrix. This makes it very difficult to calculate and store $\mathbf{B}$ or it's inverse matrix $\mathbf{B}^{-1}$.

The cost function is minimized using conjugate gradient software based on CONGRAD (Fisher [1998]). The specific minimization algorithm used in the V2 hindcast was CGMOD where a B preconditioning is applied in the conjugate gradient minimisation.

3 Multivariate Balance

An attractive feature of NEMOVAR is the balance relationships which allow us to account for the correlations between ocean variables. These balance relationships are defined through the balance operator K. The idea is that the ocean variables can be rewritten as the sum of balanced and unbal-

© Crown Copyright 2013

anced components. The inverse operator K^{-1} transforms the vector of mutually correlated variables $\delta\mathbf{x} = (\delta T, \delta S, \delta\eta, \delta\mathbf{u}, \delta C)$ into a vector of unbalanced variables, $\delta\mathbf{x}_U = (\delta T, \delta S_U, \delta\eta_U, \delta\mathbf{u}_U, \delta C_U)$. The linearised balance relationships for the increments defined by Weaver et al. [2005] are written below. Weaver et al. [2005] chose temperature as the lead variable and therefore temperature is treated in totality throughout.

$$\begin{aligned}
\delta T &= \delta T \\
\delta S &= K_{ST}\delta T + \delta S_U \\
\delta\eta &= K_{\eta\rho}\delta\rho + \delta\eta_U \\
\delta u &= K_{up}\delta p + \delta u_U \\
\delta v &= K_{vp}\delta p + \delta v_U \\
\delta C &= \delta C_U
\end{aligned} \tag{2}$$

where the density increment, $\delta\rho$ and the pressure increment δp are defined as follows

$$\begin{aligned}
\delta\rho &= K_{\rho T}\delta T + K_{\rho S}\delta S \\
\delta p &= K_{p\rho}\delta\rho + K_{p\eta}\delta\eta
\end{aligned} \tag{3}$$

The balanced density equation is the linearised equation of state, while the balanced pressure equation is the vertically integrated hydrostatic equation. The operator K_{ij} denotes the transformation from the variable j to i. We have extended the state vector to include sea ice concentration. This is currently treated as a totally unbalanced variable in the linearised balance relationships.
A brief description of each component of K is given below. For a more detailed description of the balance relationships refer to Weaver et al. [2005] and Mogensen et al. [2012].

Salinity balance, K_{ST}

The temperature-salinity balance is a linearised version of the water-mass property conservation scheme of Troccoli and Haines [1999]. The assumption is that the Temperature-Salinity relationship in the water column is preserved. In NEMOVAR the salinity balance relationship is defined by $K_{TS} = \frac{dS}{dT}$, where this gradient is calculated from the model background field.
In our implementation of NEMOVAR we smooth K_{TS} using the diffusion operator with the horizontal temperature lengthscales. This is because the $\frac{dS}{dT}$ fields tend to be quite noisy which results in noise in the balanced salinity increments. It also seems physically consistent for the temperature-salinity relationship to vary slowly over the region of the temperature lengthscales.

© Crown Copyright 2013

SSH balance, $K_{\eta\rho}$

The balanced component of SSH is a baroclinic term which depends on density. The baroclinic component can be estimated from:

$$\rho_0 \delta\eta_B = -\int_{z=-H}^{0} \delta\rho(z')dz' \tag{4}$$

where η_B denotes the balanced SSH, H is the reference depth which is set to 1500m in NEMOVAR and ρ_0 is a constant reference density. The assumption of a level of no motion is not ideal and may be revisited in future implementations. The balanced component should be small in regions of low stratification and therefore the temperature and salinity increments associated with the SSH balance should be focused below the mixed layer depth. However, the inverse of the SSH balance relationship is ill-posed and we found that the temperature and salinity increments related to the SSH balance were too large in the mixed layer. We have therefore adjusted the SSH balanced equation so that

$$\rho_0 \delta\eta_B = -\int_{z=-H}^{z=zmld} \delta\rho(z')dz' \tag{5}$$

where $zmld$ is the mixed layer depth. This ensures that there is no spurious SSH balance above the mixed layer depth. In our implementation of NEMOVAR the mixed layer depth is consistently defined by the mixed layer depth of Kara et al. [2000].

Within NEMOVAR there is an option to apply a latitude cut-off for SSH balance which was implemented to prevent the SSH balance being applied at geographical locations where vertical stratification is low. We have implemented an alternative cut-off which is purely stratification dependent. When the temperature difference between the surface and bottom is less than 5 degrees, no SSH balance is applied. If the temperature difference is more than 10 degrees then the full SSH balance is applied and if it is between 5 and 10 degrees a linear ramp is applied. This ramp is based on the scheme applied in FOAM-AC.

Velocity Balance, K_{up}, K_{vp}

In the present implementation of NEMOVAR, current data are not assimilated and there are therefore only balanced velocity increments. The balanced velocties are assumed to be in geostrophic balance. The geostrophic balance is proportional to the balanced pressure divided by the coriolis parameter and is refered to as the f-plane velocity balance. Close to the equator this becomes unbounded and thus the β-plane approximation is applied instead. The β-plane velocity balance includes the second order meridional derivative of the pressure increments. An exponential function is used to weight the f-plane and β-plane balance. The weights W are defined so that $W_f = 1 - W_\beta$, $W_f = 0$ at the equator and increases to 1 away from the equator. The β-weight is defined by Weaver et al. [2005] as $W_\beta = exp(-\phi^2/2L_\beta^2)$ where ϕ denotes latitude and $L_\beta = 1.55$ is a lengthscale whose size is based on the Rossby radius of deformation.

© Crown Copyright 2013

In the $\frac{1}{4}$ degree model we found that the β-plane velocity balance is very sensitive to the magnitude of the gradients in the temperature and salinity increments. This has some dependency on the background error lengthscales for the temperature and salinity (longer lengthscales reduce the problem). However, even with the relatively long lengthscales of the equatorial region described later, the gradients in the temperature and salinity increments were still large enough to cause very large velocity increments. We have therefore found it necessary to remove the β-plane balance in our initial implementation.

The exponential ramping used to determine the balance weights was also found to cause a problem in ORCA025. The f-plane weights are non-zero one grid point from the equator and this results in f-plane balanced velocity increments at $\frac{1}{4}$ degree North and South. These near equatorial velocity increments can be quite big. In a hindcast run of several months these velocity increments generated large currents and spurious equatorial waves in the Western Tropical Pacific. This eventually resulted in large errors in the temperature, salinity and SSH fields. We have therefore chosen to redefine the weights using a linear ramp. The weights W_f are set to zero between 1 degree North and South and then linearly ramped to 1 at 5 degrees North and South. This new ramping has overcome the problems seen in the Tropical Pacific. Figure 1 compares zonally averaged U increments when using the exponential and linear ramps. We see from this plot that applying the linear ramp prevents the large spike in the increments near to the equator. There are, however, some questions about whether this approach is consistent with the way the second order balance is defined. Consequently, the form of the equatorial ramp will be revisited in the future.

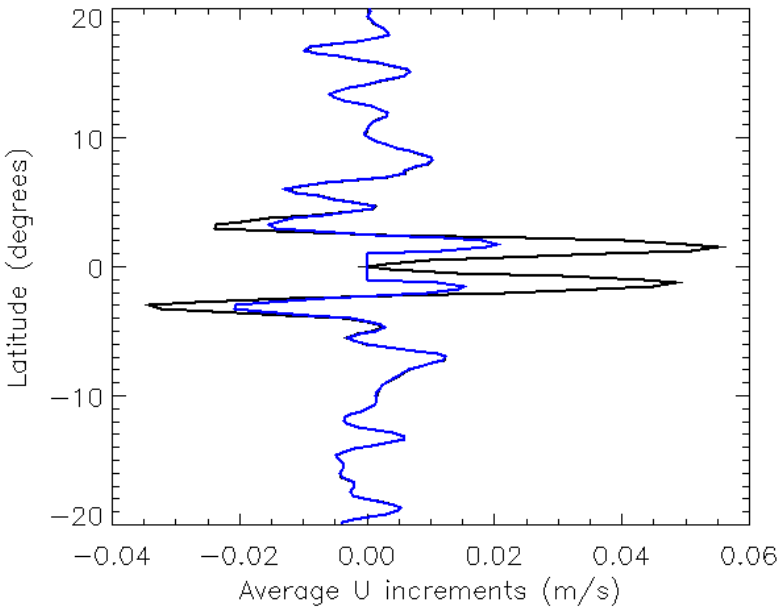

Figure 1: An example of zonally averaged U increments (m/s) for one day plotted against latitude for once day. The black line is the averaged increments using the exponential equatorial ramp, the blue line in the averaged increments using the new linear ramp.

© Crown Copyright 2013

4 Background Error Covariances

Modelling and evaluating the background error covariances is one of the most complex components of a data assimilation scheme. Statistical methods, empirical models or knowledge of physical processes are generally used to determine variances and a correlation model with appropriate lengthscales.

In NEMOVAR the full multivariate background error covariance matrix $\mathbf{B}$ can be written as a combination of the univariate background error covariance matrix $\mathbf{B}_U$ and the balance operator $\mathbf{K}$,

$$\mathbf{B} = \mathbf{K}\mathbf{B}_U\mathbf{K}^T \tag{6}$$

where $\mathbf{B}_U$ is a block diagonal matrix, with each block containing the covariances of the mutually uncorrelated variables $(T, S_U, \eta_U, \mathbf{u}_U, C_U)$. We will refer to $\mathbf{B}_U$ as the unbalanced background error covariance matrix

The unbalanced background error covariance is rewritten as follows

$$\mathbf{B}_U = \mathbf{D}^{1/2}\mathbf{F}\mathbf{D}^{1/2}, \tag{7}$$

where $\mathbf{D}^{1/2}$ is the diagonal matrix of standard deviations and $\mathbf{F}$ the block diagonal matrix of correlations. Therefore for each unbalanced model variable it is necessary to define the background error standard deviations and a background error correlation model. Since temperature is treated in totality within the balance relationships, we determine the complete temperature background errors. The same is done for sea ice which is treated as a univariate variable. Meanwhile, for salinity and SSH we need to specify background errors for the unbalanced component exclusively.

Before describing the background error covariances used in the FOAM-NEMOVAR system we will give an overview of the background errors implemented in FOAM-AC. The FOAM-AC background errors are seasonally varying statistical errors. They were calculated using the NMC method (Parrish and Derber [1992]) from 2 years of data with the variances being scaled using values generated by the Hollingsworth and Lonnberg method (Hollingsworth and Lonnberg [1986]). The calculation of the FOAM-AC errors was separated into four seasons to capture the seasonal variations. A Second Order Auto Regressive (SOAR) horizontal function with two lengthscales was fitted to the NMC statistics at all global locations. The two lengthscales were fixed at 40km and 400km. These lengthscales were chosen to represent the small scale (mesoscale) and large scale (synoptic) processes. The function fitting produced fields of mescoscale and synoptic scale NMC variances. A more detailed description of the FOAM-AC errors can be found in Martin et al. [2007]. In this implementation of FOAM-NEMOVAR we are using a single horizontal correlation lengthscale in the error covariances. Therefore, unless otherwise specified, the FOAM-AC background error standard deviations/variances discussed below are the total of the mesoscale and synoptic scale components.

© Crown Copyright 2013

The specification of the standard deviations and correlations within our implementation of NEMOVAR are described in sections 4.1 and 4.2. Much of the work has focused on developing background errors which are both temporally and spatially varying. Temporally varying background errors have the advantage that they are able to evolve with changes in the physical situation. This means that they are better able to model the errors at a particular time and location. In an ensemble system, the evolution of the errors can be estimated and updated using ensemble statistics. However, for our variational system non-static background errors are achieved by parameterising the change in the background error standard deviations and correlations based on knowledge of the physical processes. This may not capture all the spatial (and temporal) variability in the errors, it is therefore also useful to consider climatological error covariances calculated from statistical methods. The climatological error covariances can provide us with information on the 3D spatial variation of the background errors, which can highlight regions and situations where larger errors occur. Generating spatially varying background errors ensure that the errors reflect the areas which are difficult to accurately model.

4.1 Background Error Standard Deviations

For our implementation of NEMOVAR we have attempted to combine the existing vertical parameterisations for temperature and salinity with our FOAM-AC statistical background errors to achieve both spatially and temporally varying background errors. We will begin by describing the original parameterisation in NEMOVAR and then discuss our developments to this at the Met Office.

Original Temperature Background Error Parameterisation

In NEMOVAR the default temperature background error standard deviations are parameterised based on the vertical temperature gradients, which results in flow dependent errors (Daget et al. [2009] and Weaver et al. [2003]). The parametrisation is specified as follows:

1. The temperature depth gradient field $\frac{dT}{dz}$ is calculated from the background fields
2. The depth, d_{ml}, at which the maximum value of $|\frac{dT}{dz}|$ occurs is calculated. If the maximum occurs below 300m, d_{ml} is set at 300m
3. The vertical gradient field is multiplied by a vertical positioning error δz, such that the temperature background error standard deviations $\sigma_T = \delta z \frac{dT}{dz}$. Where the error exceeds the specified maximum error, σ_{max}, it is set to σ_{max}. A lower bound σ_{ml} is set above d_{ml} and a lower bound σ_{do} is set below d_{ml} in the deep ocean
4. Finally a horizontal smoothing is applied.

© Crown Copyright 2013

We have compared the parameterised errors to statistical errors for ORCA025 with 50 levels. The NMC method (Parrish and Derber [1992]) was used to calculate statistical background errors from 1 month of 24 hour and 48 hour forecast temperature fields. The chosen month is January 2007. For the parameterisation we set $\sigma_{max} = 2.5K$, $\sigma_{ml} = 0.5K$, $\sigma_{do} = 0.07K$ and $\delta z = 10m$. The 24 hour forecast temperature fields were used to calculate the parameterised background errors at each day and these were then averaged over the month. We then compared the profile shape of the parameterised and statistical errors. Figure 2 shows a comparison of the profiles of the background error standard deviations at 170W 0N. The magnitudes are quite different, but this is because the NMC method is known to underestimate the errors and normally requires rescaling. However, the general shape of the two profiles is very similar. Figure 3 shows the correlations between the vertical structures in the NMC and parameterised errors and gives a more global view of how well they compare. From this plot we generally see good correlations, particularly in the Northern Pacific. Some areas show lower correlations but these tend to be coastal regions where there are fewer observations (which will impact on the quality of the NMC errors) and high latitude regions where the water column is less stratified. However, in general the structure of the NMC and parameterised errors appears to compare well.

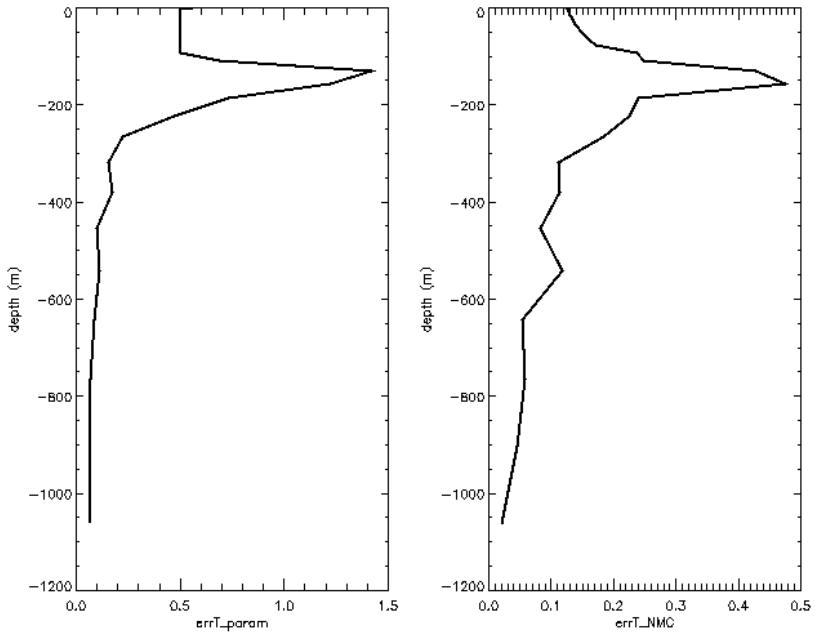

Figure 2: Temperature background error (K) profiles at 170W 0N. Left hand plot shows the errors calculated from the parameterisation while the right hand plot shows the errors calculated by the NMC method. Both are calculated using data from January 2007.

We also compared the impact of using the parameterised and background errors on the model statistics. Table 1 shows the temperature and salinity profile RMSE (root mean square error) calculated from the difference between the model background field and the observations prior to assimi-

© Crown Copyright 2013

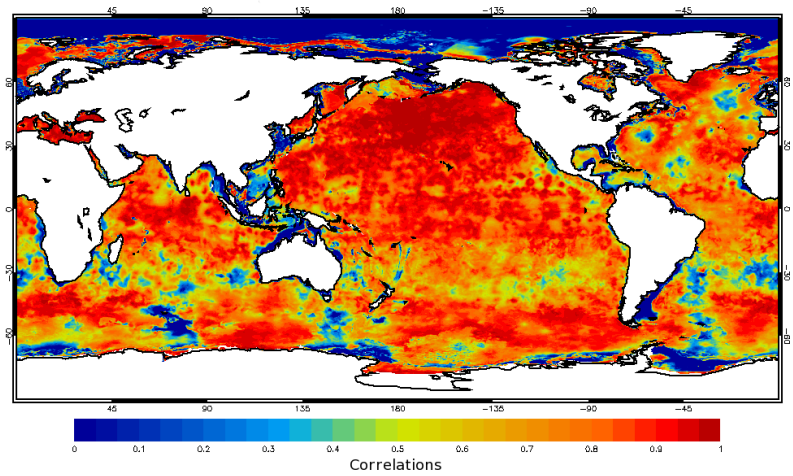

Figure 3: Vertical correlations between NMC and parameterised errors for January 2007.

lation. The results are from 15 day hindcast runs with NEMOVAR in ORCA025 with 50 levels. The results shown are for a free model run, for an assimilation run using the parameterised temperature background error standard deviations and an assimilation run using the FOAM-AC temperature background error standard deviations. The statistics show that there are better results for both temperature and salinity when using the parameterised background error.

Overall, we have shown that the parameterised errors generally compare well to the NMC errors, but they have the advantage of being flow dependent so they can better represent temporal variability in the fields. They also produced better results in our test run and we have therefore chosen to use the parameterised errors. However, we have incorporated some changes to the parameterisation.

Table 1: Profile RMSE

	No assimilation	param T background errors	NMC T background errors
T prof RMSE	0.733	0.667	0.771
S prof RMSE	0.160	0.148	0.151

4.1.1 Met Office Temperature Background Error Parameterisation

In our implementation of NEMOVAR we have set the scaling parameter δz equal to 20m. This value was chosen after comparing the profiles of the parameterised errors to the FOAM-AC errors. In future developments we may include globally varying δz.

The parameterisation has the advantage that it is flow dependent but since it is a vertical parameterisation it does not account for the horizontal variability of the background errors. We first tried to account for the horizontal variability by setting σ^T_{ml} equal to the value of the FOAM-AC surface temperature background error standard deviations. The deep ocean lower bound, σ^T_{do}, was set to 0.07.

© Crown Copyright 2013

While assimilation results showed good improvements near the surface, the subsurface results were quite poor. It was found that the assimilation was barely fitting the analysis to the observations at depth. This was because below the mixed layer the parameterisation tends to converge quickly to the deep ocean lower bound and since this value is small, the observations have relatively low weight. We have therefore chosen to replace the two lower bounds, σ^T_{ml} and σ^T_{do}, with a continuous function, σ^T_{do}, which smoothly decreases from the FOAM-AC surface temperature background error (σ^T_{surf}) at the surface to the FOAM-AC temperature background error lower bound which is 0.098. The chosen function is defined as follows:

$$\sigma^T_{min}(i,j,k) = 0.098 + (\sigma^T_{surf}(i,j) - 0.098)\exp\left[\frac{d(1)-d(k)}{500}\right] \tag{8}$$

where d is the level depth and i,j,k are the indices in the E/W, N/S and vertical directions. Figure 4 shows the background errors when the old minimum is used compared to the new minimum. From this example we can see that the background errors do not converge so sharply to a minimum value. The result is that the observations will have more weight, particularly below 500m.

The final modification to the parameterisation is the application of a vertical smoothing. The diffu-

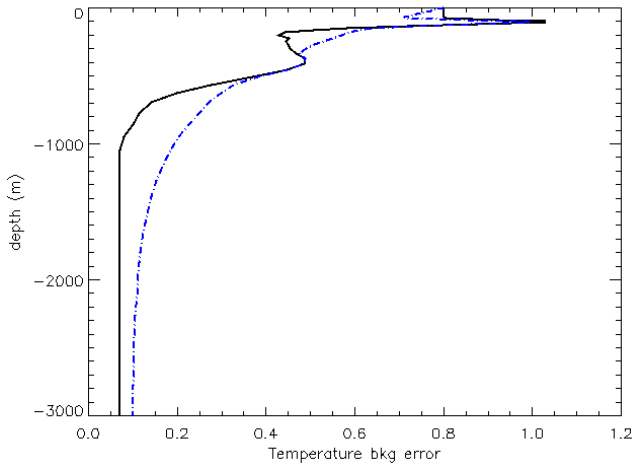

Figure 4: Temperature background error (K) at 170W 35N. The solid line shows the temperature background error when the minimum values are set by σ^T_{ml} and σ^T_{do}. The dashed line shows the results when σ^T_{min} is defined as in equation (8)

sion filter with the temperature vertical lengthscales is used to smooth the background errors. This removes the impact of noise in the vertical temperature gradients and is internally consistent since the smoothing depends on the assumed lengthscales of the temperature background errors. It also allows for errors in the position of the thermocline in the water column.

Figure 5 shows an example of a vertical profile of temperature background errors along with the surface temperature background errors for our final parameterisation. The parameterised temperature background errors in the profile plot peak at the thermocline and then reduce with depth, this compares well with the FOAM-AC errors. Meanwhile the surface plot shows the horizontal variability

© Crown Copyright 2013

in the errors, with larger errors in regions of high variability such as the Gulfstream.

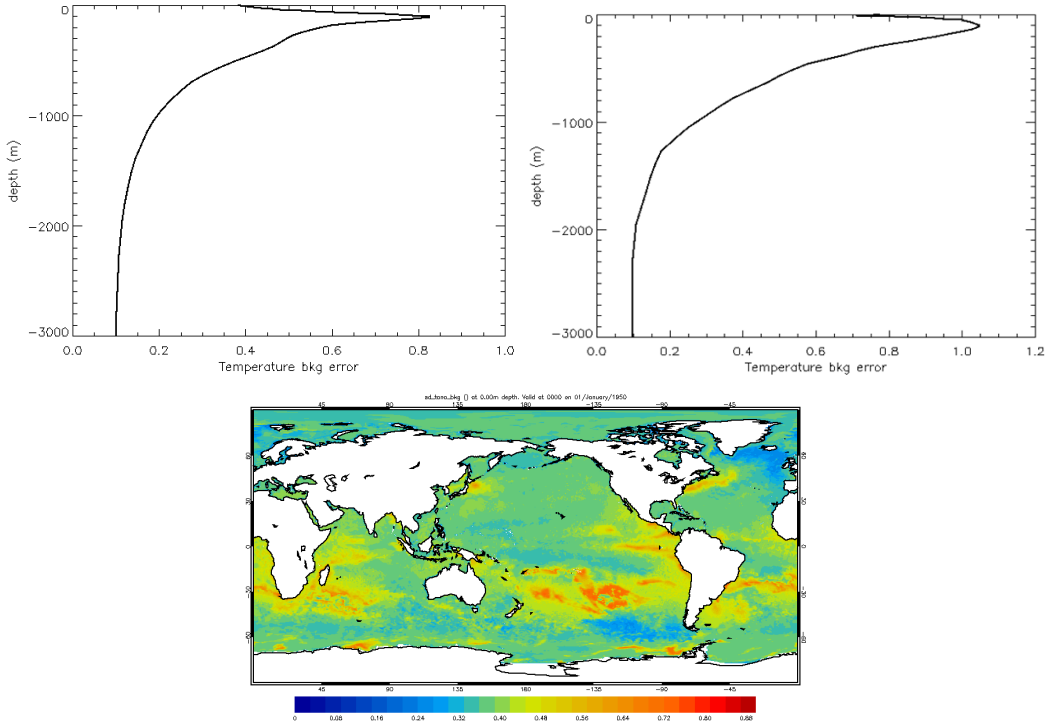

Figure 5: Temperature background error standard deviation (K). Top left hand plot shows a profile of the parameterised errors at 170W 35N, top right hand plot shows a profile of the FOAM-AC errors at 170W 35N, bottom plot shows the surface background errors for the parameterised errors

4.1.2 Salinity Background Errors

When considering the salinity and SSH background error we need to specify errors which only represent the unbalanced component. The default NEMOVAR background error standard deviations for salinity are vertically parameterised based on the $\frac{dS}{dT}$ field (Daget et al. [2009]). The depth at which $|\frac{dS}{dT}|$ is maximum is determined, and it is assumed that this depth corresponds to the bottom of the density mixed layer. The unbalanced salinity background error is then set to a maximum value, σ^S_{max}, above this level. If the maximum $|\frac{dS}{dT}|$ occurs below depths of 200m the bottom of the mixed layer is set at 200m. Below the determined mixed layer depth the unbalanced salinity background error is set to a minimum value σ^S_{min}. A transition region is also specified to allow a smooth transition between the unbalanced salinity background error standard deviation of the mixed layer and that below. The physical justification for the parameterisation is that above the density mixed layer depth the temperature and salinity errors are assumed to be unbalanced and therefore the unbalanced errors dominate. Below the mixed layer temperature and salinity are assumed to be primarily in balance and thus unbalanced errors are small.

© Crown Copyright 2013

We have modified the original parameterisation to included horizontal variability in the background errors using the FOAM-AC background errors. The method has been altered so that σ^S_{max} is set equal to the FOAM-AC salinity surface background error standard deviations. Once the background error standard deviations have been calculated they are smoothed horizontally using the diffusion equation. This is to avoid noise in the salinity, balanced velocity and balanced SSH increments.

4.1.3 SSH Background Errors

For the SSH background errors we use only the synoptic component of the FOAM-AC SSH background errors. We assume that a large proportion of the synoptic scale errors is barotropic and therefore associated with the unbalanced SSH background errors. Figure 6 shows the December-January-February (DJF) SSH background error standard deviations. The errors were rescaled by a factor of 0.276 to make their magnitude consistent with the implied balanced background errors. This scaling factor was derived by applying the linearised balance operator to the temperature and salinity background error standard deviations (for one day) to determine an implied balanced SSH background standard deviation. The mean of this background error was calculated and compared to the mean of the mesoscale SSH background error standard deviation. The ratio of the two means was then determined and used as the scaling factor for the synoptic scale errors.

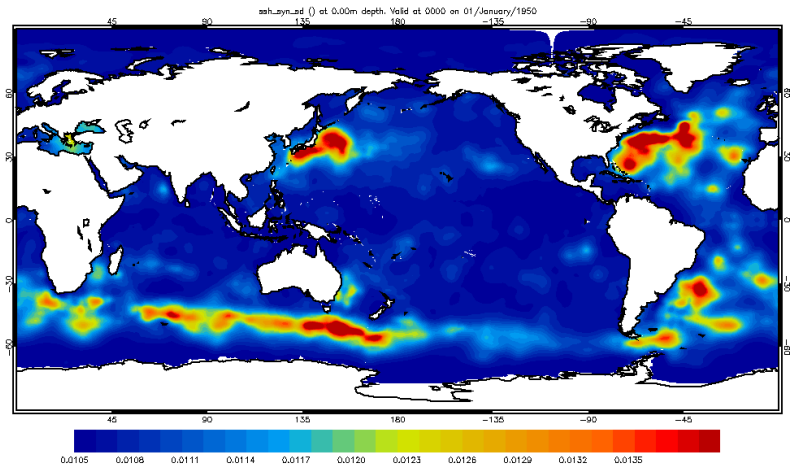

Figure 6: DJF SSH background error standard deviations

4.1.4 Sea Ice Concentration Background Errors

The sea ice concentration background errors used in FOAM-NEMOVAR are the same as the FOAM-AC background errors. Figure 7 shows the DJF sea ice concentration background error standard deviation in the Arctic and Antarctic. In the Arctic the largest errors are in the marginal ice zone.

© Crown Copyright 2013

The errors are generally large throughout the domain in the Antarctic, this may be because these errors are for the Southern hemisphere summer when melt ponds are present.

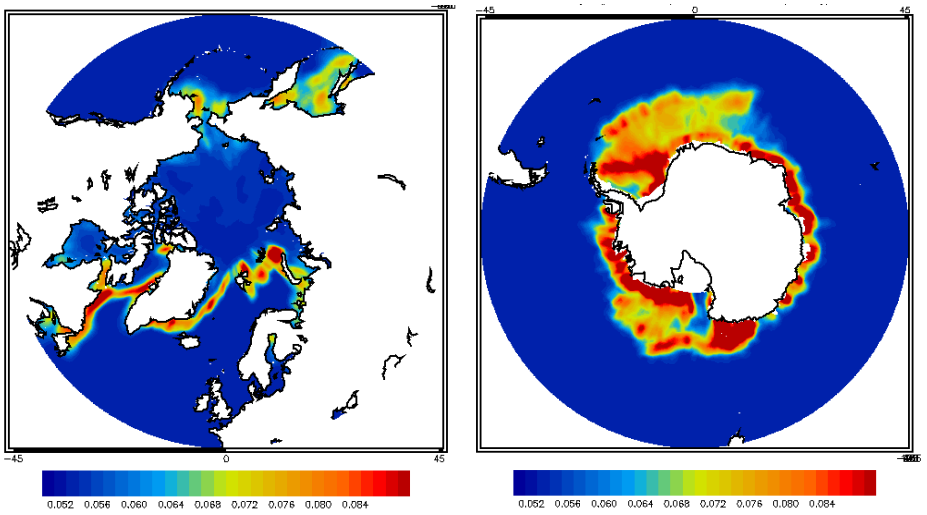

Figure 7: Northern hemisphere winter sea ice concentration background error standard deviations. Right hand plot is the Arctic and left hand plot is the Antarctic.

4.2 Background Error Correlations

For large atmospheric and ocean models it is not possible to explicitly evaluate the correlation matrix due to its size. In variational schemes the background error correlations are generally parameterised using statistical functions, such as Gaussian or auto regressive functions. This has led to the development of various methods for representing correlation models. Some of these methods parameterise correlation matrices using smoothing functions or filters. In the FOAM-AC system a recursive filter is used to model a SOAR function (Martin et al. [2007]). The recursive filter (Purser et al. [2003]) efficiently models correlation functions and can allow for geographical variations but has difficulty in achieving isotropic correlations when applied in 1D. In NEMOVAR the background error correlations are modeled using the diffusion equation. Successive applications of a diffusion operator are applied to simulate the matrix multiplication of a Gaussian correlation matrix. The method is easily generalized to account for complex boundary conditions, can be extended to model various different auto-regressive functions and allows for geographically varying lengthscales (Weaver and Courtier [2001]). Two methods have been implemented within NEMOVAR, an explicit diffusion operator (Weaver and Courtier [2001]) and an implicit diffusion operator (Mirouze and Weaver [2010]). The explicit diffusion operator is applied as a 2D horizontal correlation function and a 1D vertical correlation function. In the explicit diffusion model a large number of iterations are required to ensure stability. This is very costly and since the number of necessary iterations increases with the ratio of lengthscales to grid size, this restricts the magnitude of the lengthscales which can practically be applied. Within ORCA025 it was necessary to restrict horizontal length-

© Crown Copyright 2013

scales to around 0.5 degrees (only twice the grid resolution) to achieve a reasonable computational cost.

The implicit diffusion method is unconditionally stable and thus computationally cheaper to apply than the explicit scheme. This allows much more freedom in the way the correlation lengthscales are defined. However, defining 2D and 3D implicit diffusion correlation operators is complicated and only 1D implicit diffusion operators are currently available in NEMOVAR. Applying three 1D diffusion operators can cause problems near islands and in coastal regions. We have found that horizontal lines can be created through islands and along coastlines and that these are related to the direction of the last sweep of the diffusion operator. This problem can be mitigated by interleaving the application of the diffusion operator along the x- and y- directions (which increases computational cost) or by reducing the correlation lengthscales near the coast. Despite this drawback the implicit scheme remains the only viable option for high resolution models (such as ORCA025) and is therefore the chosen scheme for this implementation.

Horizontal Correlation Lengthscales

The horizontal error correlation lengthscales for temperature, salinity and sea ice concentration are dependent on the Rossby radius, similar to Cummings [2005]. The Rossby radius represents the lengthscales of the oceans' mesoscale processes. The Rossby radius also produces quite short lengthscales in most regions and assimilating with these lengthscales is less likely to cause the kind of instabilities which can be created when crossing gradients of potential vorticity. The Rossby radius was calculated from a 1 year average of temperature and salinity fields from a previous run of FOAM-AC. We have also included code in NEMOVAR to calculate the instantaneous Rossby radius. This is not suitable for our application because it complicates the calculation of the normalisation factors (this is discussed further below). We also found that the Rossby radius does not vary significantly in time and therefore an annual average is a good approximation. Outside the equatorial region the Rossby radius is calculated using the following equation,

$$\lambda_m(\lambda,\phi) = \frac{0.4}{|f|} \int_H^0 N(\lambda,\phi,z)dz \tag{9}$$

where $f = 2\Omega \sin\phi$ is the Coriolis parameter and N is the buoyancy frequency. The dependence of the Rossby radius on $1/f$ becomes a problem near the equator and therefore the Rossby radius has been capped at 300km. This maximum cap is generally reached at around 5 degrees from the equator. It is also necessary to set a minimum value (here 25km) since the lengthscales should not be smaller than the grid resolution in order to maintain numerical stability of the diffusion operator. A global plot of the calculated Rossby radius is shown in Figure 8.

It is assumed that the zonal lengthscales will be longer than the meridional component near the equator due to spreading of information by the dominant East-West currents. We model this by reducing the maximum cap in the meridional lengthscales to 150km and this produces elliptical in-

© Crown Copyright 2013

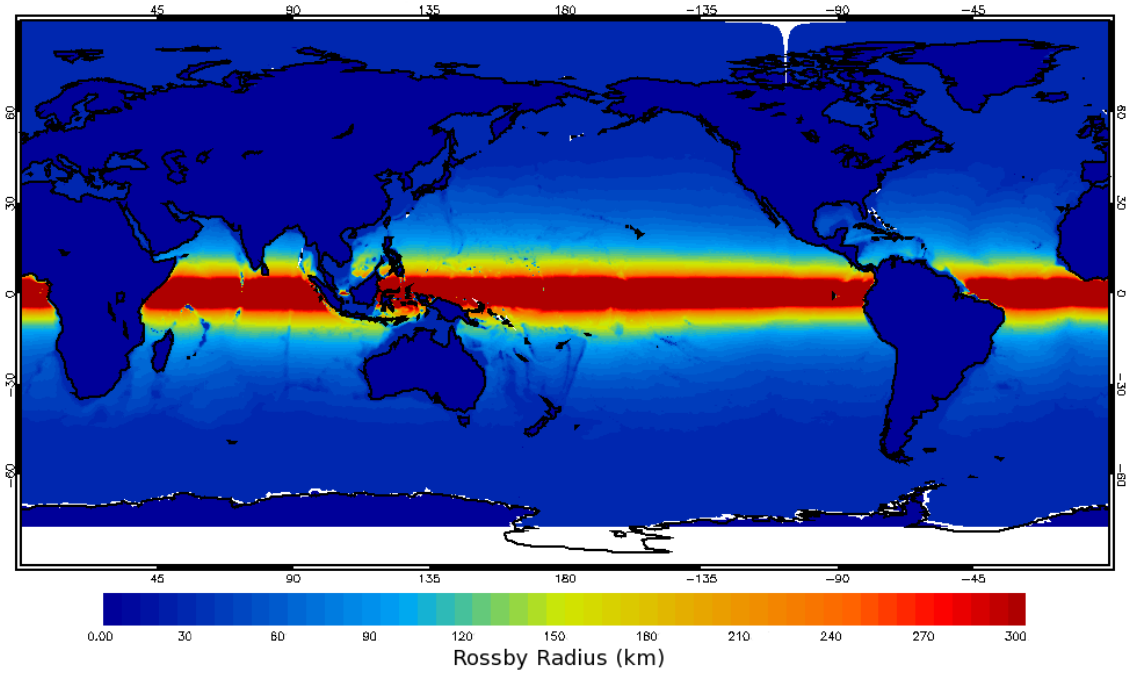

Figure 8: The Rossby radius.

crements near to the equator and circular increments at higher latitudes. Figure 9 shows the zonally averaged horizontal lengthscales

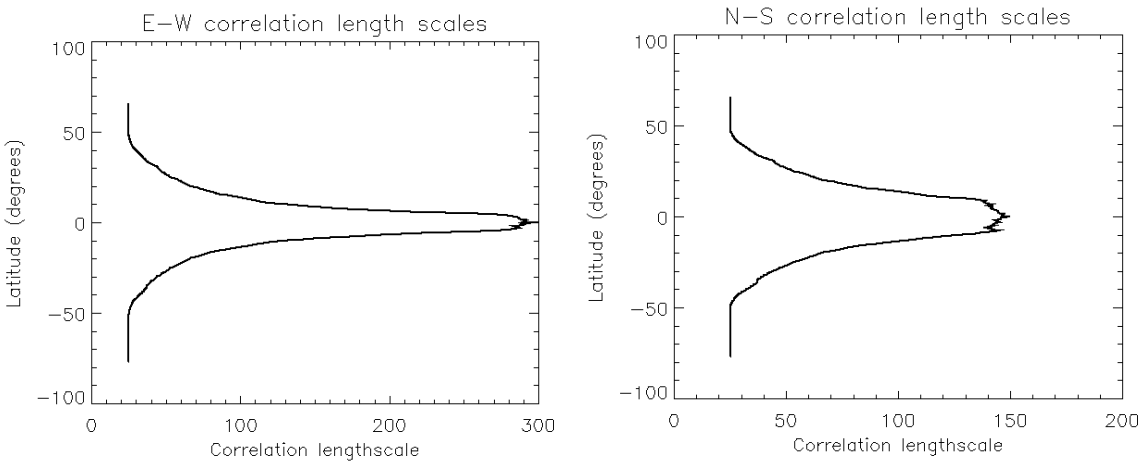

Figure 9: Zonally averaged horizontal lengthscales (km).

While the temperature, salinity and sea ice concentration background error lengthscales depend on the Rossby radius and represent the mesoscale processes, much longer lengthscales are defined for the unbalanced SSH background error to represent the barotropic errors. The lengthscales are chosen as 4 degrees everywhere, which is similar to the 400km synoptic scales used in FOAM-AC. The issues of horizontal lines through islands and along coastlines in the increments was discussed above. The problem is particularly apparent when the lengthscales are quite long (ie. everywhere for the SSH and in the Tropics for temperature and salinity). One of the potential solutions is to

© Crown Copyright 2013

reduce the correlation lengthscales near the coast. This has been applied in our FOAM-NEMOVAR implementation. The temperature, salinity and sea ice concentration lengthscales are linearly reduced from their value at 150km distance from the coast, to 25km at the coast. For SSH the same linear ramping is applied, but from 600km from the coast. This significantly reduces the problems with the increments. In the future the ramping down of correlation lengthscales scales near to the coast may be replaced with, or applied along side interleaving. This will be investigated to ascertain the effectiveness and added computational cost.

Vertical Correlation Lengthscales

The vertical lengthscales in FOAM-NEMOVAR have the same structure for both profile and SST assimilation. This is in contrast to FOAM-AC where the SST and profiles were assimilated separately using different background error covariances. In FOAM-AC the vertical lengthscales for the SST background error correlation were designed to project the SST increments to the bottom of the mixed layer. This was done rather crudely by projecting the increments with a correlation of one down to the base of the mixed layer and a correlation of zero below that. The assumption is that while the ocean is well mixed, the errors will be strongly correlated. However, there are some practical disadvantages to this scheme. The mixed layer depth is determined from the background field, so any errors in the background mixed layer depth will be reinforced by the SST assimilation applying large increments above the background mixed layer depth and no increments below it. For the FOAM-AC profile assimilation there are two vertical lengthscales. A 100m vertical lengthscale is used for the synoptic scale component and a 200m vertical lengthscale for the mesoscale component. These lengthscales are constant with depth.

The default vertical lengthscales in NEMOVAR are defined as a multiple of the grid resolution. The grid size near the surface is approximately 1m and is more than 200m near the bottom of the ocean. If we consider the lengthscales at the bottom of the water column, a factor of 2 may be sensible since the vertical grid resolution is determined based on scales of variability. However, this only allows a lengthscale of 2m near the surface which significantly limits the vertical projection of the SST information. The effect of this is that the SST assimilation has very little impact. An alternative to this scheme could be the implementation of constant vertical lengthscales but since the lengthscales should be at least the grid resolution, this limits us to using constant vertical lengthscales of more than 200m.

Cummings [2005] used vertical lengthscales which are inversely dependent on the vertical pressure gradients. The lengthscales are therefore short in highly stratified regions (i.e the thermocline) and long in unstratified regions (ie. the mixed layer and deep ocean). An example of density dependent lengthscales is shown in Figure 10. Some of the difficulties with applying Cummings [2005] method are choosing a suitable factor for scaling the inverse vertical density gradients and applying a sensible cap for regions where the density gradients are very small. When we applied the method we found that it was difficult to find an appropriate value for capping large values and that the length-

© Crown Copyright 2013

scales were sensitive to very small scale features in the density gradients.

As an alternative we have decided to parameterise the background error vertical correlation length-

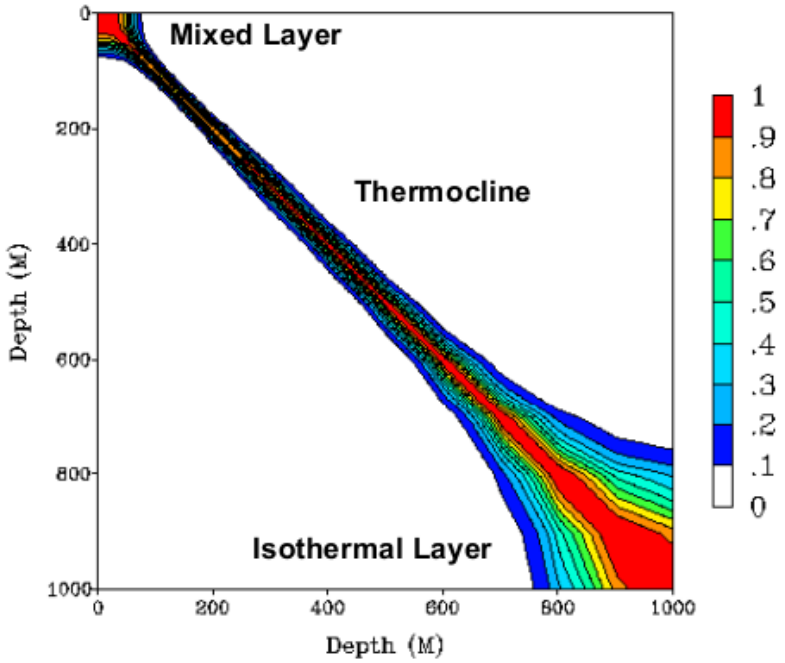

Figure 10: Vertical correlations as a function of depth (Cummings [2003])

scales in a way that captures the key features of Cummings [2005] lengthscales. The parameterisation has been designed so that the lengthscales are large enough at the surface to project SST increments through the mixed layer but shorter in the highly stratified region of the thermocline. At the surface the vertical lengthscales are set as the mixed layer depth of the background field and then linearly decrease to $2\beta(kmxl)$ at the mixed layer depth, where $kmxl$ denotes the k index associated with the mixed layer depth. Below the mixed layer depth the vertical lengthscales are set equal to $2\beta(k)$. The function $\beta(k)$ is defined as follows:

$$\beta(k) = \quad 103.95 + 2.43 \tanh\left(\frac{k-15.35}{7.}\right) 100.76 \tanh\left(\frac{k-48.03}{13.}\right)\Bigg] \tag{10}$$

This is the same function used to define the vertical mesh length for the 75 level version of NEMO. The parameterisation is chosen to converge to 2β as this ensure conditional stability for the diffusion operator. Finally the lengthscales are smoothed vertically using a 5-point unweighted smoothing to produce smooth transitions of the lengthscales in the thermocline. Figure 11 shows an example of the vertical lengthscales when the mixed layer depth is 100m. These parameterised lengthscales still depend on the background fields but since they are smoothly varying they shouldn't reinforce wrongly positioned mixed layer depths so strongly. There is, however, the possibility that they may spread information to beneath the mixed layer which could lead to spurious mixing and degrade the mixed layer depth. They are also unaffected by spurious noise in the density fields but are able to

© Crown Copyright 2013

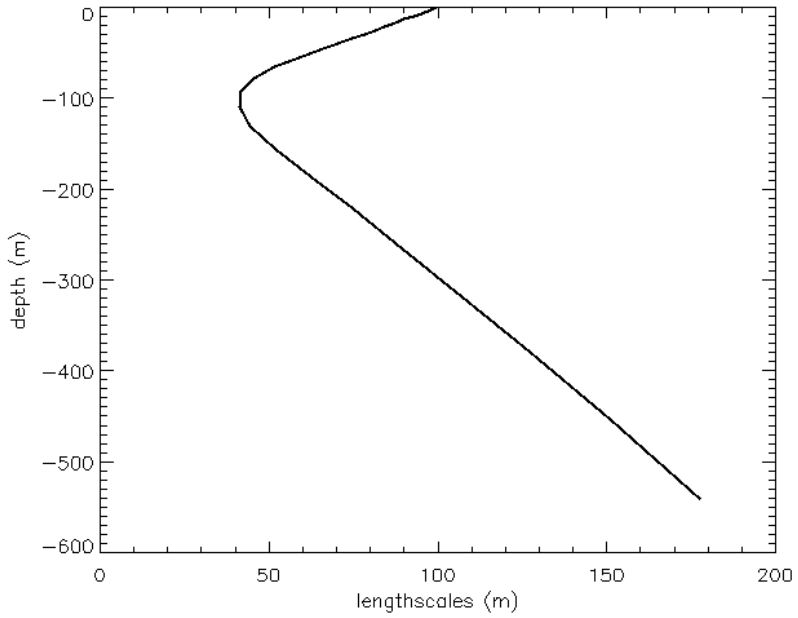

Figure 11: Parameterised vertical lengthscales for a mixed layer depth of 100m

provide flow dependency to the vertical lengthscale specification. Furthermore, the same lengthscales can be used consistently for all temperature data (SST and profile data).

Normalisation Factors

While there are clear advantages to using temporally varying lengthscales there are also some difficulties in the practical application. These are primarily related to the normalisation factors. Once the diffusion operator has been applied it is necessary to multiply the field by a diagonal matrix of normalisation factors which generate Autoregressive correlations. Calculating the normalisation factors is a non-trivial and computationally expensive task.

For the implicit diffusion operator, the analytical normalisation factors for a Gaussian function are defined as

$$\lambda = \sqrt{2\pi} L_g \tag{11}$$

where L_g is the Daley lengthscale (see (Mirouze and Weaver [2010])). The analytical solution provides an approximation to the exact normalisation factors and Mirouze and Weaver [2010] showed that this is a good approximation when the lengthscales are constant or varying slowly. However, our parameterisation of the vertical lengthscales produces fairly rapidly varying lengthscales in the mixed layer and this results in large errors in the correlations when the analytical normalisation factors are applied. It was also found that the errors tend to be a consistent over-estimation or underestimation at a particular depth. Applying these normalisation factors would therefore cause biases in the increment field. A similar issue would arise if we used Cummings [2005] density

© Crown Copyright 2013

dependent lengthscales or any other lengthscales which vary rapidly in space. One possible solution would be to calculate the exact normalisation factors but this is equivalent to applying N applications of the diffusion equation, where N is the number of grid points. This would be far too computationally expensive to apply for realistic ocean models. A more affordable alternative is to use the randomisation method, Weaver and Courtier [2001]. The randomisation method calculates the normalisation factors by applying the generalised diffusion operator to an ensemble of random vector fields. This method can produce more accurate results than the analytical method when lengthscales vary rapidly, but requires a sufficiently large ensemble size. For ORCA025L75 an ensemble of 3000 members has been chosen to balance computational resources and accuracy. On 128 processors it takes around 4 hours to calculate the normalization method for 3000 members. It is therefore not practical to recalculate the normalisation factors at each analysis time-step. For the case where correlation lengthscales are stationary this is not a problem, and normalisation factors can simply be calculated once. However, it is important that in our system the vertical lengthscales can vary with local conditions, and therefore it is necessary to seek an alternative method.

We have implemented a normalisation look-up table in NEMOVAR. Dobricic and Pinardi [2008] used a look-up table to generate horizontal normalisation factors for a global ocean model with latitudinally varying grid resolution. They calculated the exact normalisation factors for a discrete number of grid distances and then used these to interpolate to the correct normalisation factor for each grid location. Here the look-up table is applied to allow for variable vertical lengthscales and is implemented in a slightly different way. We begin by limiting the number of vertical lengthscale parametrisations. This is done by allowing only a finite number of mixed layer depths for our vertical parameterisation. In our ORCA025L75 implementation we allow 41 different mixed layer depths and these are coincident with the depths of the top 41 vertical levels of the model, with the deepest level falling just above 600m (at 565m). We fix the mixed layer depth at one level for all global locations and calculate the vertical lengthscales using the parameterisation described above. We then calculate the normalisation factors for this level using the randomisation method with 3000 ensemble members, this process is then repeated for all the other discrete levels. At the end of this process we have created 41 files each containing normalisation factors corresponding to one of 41 mixed layer depths and this gives us our look-up table.

When we apply this look-up table in the assimilation we begin by calculating the mixed layer depth at each grid point, this field is then smoothed using a Shapiro filter. The filtering is performed to ensure that the vertical lengthscales vary smoothly in the horizontal. The next step is to generate a field of mixed layer levels corresponding to the smoothed mixed layer depths. These levels are currently calculated as the model level directly above the mixed layer depth (but could be calculated as the closest level). If the mixed layer depth for a particular location is deeper than the depth of level 41, the mixed layer level is set as 41. Once a field of mixed layer levels has been determined the parameterised vertical lengthscales can be calculated at each location. The final step is then to generate a field of normalisation factors by extracting a profile of normalisation factors at each

© Crown Copyright 2013

global position from the look-up file with the corresponding mixed layer level. This generates a 3D field of normalisation factors composed of profiles from the look-up table.

It should be noted that the vertical lengthscale parameterisation described above is used for all cases unless the mixed layer depth is less than or equal to level 1. In this specific case the vertical lengthscale parameterisation is simply equal to $2\beta(k)$ at all depths.

It is important that the horizontal lengthscales used in the assimilation are the same as those used in the generation of the normalisation look-up table. It is therefore necessary to use stationary horizontal lengthscales with the look-up table method. This is part of the reason for using the annual average Rossby radius horizontal lengthscales described above.

The performance of the normalisation look-up table has been compared to that of the analytical method. For an example day the relative error in the analytical and look-up table normalisation factors were calculated relative to the randomisation method with 3000 ensemble members. The relative errors in the analytical method near the surface were typically around 50% and in some cases more than 100%. The errors when using the look-up table were smaller and more random (of the order of 10% or less). The errors tend to increase in locations where the vertical lengthscales vary rapidly over the horizontal lengthscales, in these locations the assumption of separability of the horizontal and vertical lengthscales is less applicable. This potentially limits the application of the look-up table when horizontal lengthscales are large. The resulting correlations can also have a slightly noisy structure, but these errors are assumed small compared to errors in the background error estimates. The method could further be improved by allowing more flexibility in the vertical lengthscales and interpolating the normalisation look-up table. This will be tested in future implementations. Finally, it may be beneficial to use a larger ensemble size in the randomisation method used for calculating the look-up table. However, we are currently restricted by available computational resources.

The boundary conditions of the diffusion operator applied in FOAM-NEMOVAR are the Neumann boundary conditions. Mirouze and Weaver [2010] showed that when the analytical normalisation factors are used, the average solution from the diffusion operator applied with Neumann and Dirchelet boundary conditions gives the best approximation to a Gaussian function. Using two boundary conditions does, however, increase computational cost. Furthermore, Weaver and Courtier [2001] concluded that there is lower cost associated with the Neumann boundary conditions compared to the Dirchelet boundary conditions. Since we are unable to use the analytical solution we have chosen to use the computationally cheaper Neumann boundary conditions.

4.3 Observation Errors

In our implementation of NEMOVAR the observation errors are assumed to be uncorrelated so the observation error covariance matrix is reduced to a diagonal matrix of variances. The observation

© Crown Copyright 2013

errors used in this study are the FOAM-AC errors. The spatial structure of the observation errors is determined from the mesoscale NMC errors (see section 4), these are then scaled using the observation error variance calculated from the Hollingsworth and Lonnberg method. The NMC errors are used to define the structure of the observation errors as we expect the representivity error to dominate and we assume that this will have a similar pattern to the background errors.

5 FOAM Re-Analysis System Description

Both FOAM-NEMOVAR and FOAM-AC are a global implementation of NEMO v3.2 with data assimilation and a sea ice model. They are both run with a 24 hour analysis window and use direct fluxes from the global 40km NWP model. The interface for the FOAM system includes an observation operator step which is a 24 hour free model run where the mismatch between the background and the observations are calculated at the correct observation times. This generates the innovations and constitutes the FGAT component of the scheme. The next step is the data assimilation step, where the assimilation increments are generated by either NEMOVAR or AC. The final step is the incremental analysis update which is a 24 hour model run where the increments are gradually added over several model time-steps (Bloom et al. [1996]).
The FOAM-NEMOVAR and FOAM-AC systems are implemented within the same interface and use the same forcings, but there are various differences in their configurations and these are described in Table 2.

The same observations are assimilated in FOAM-NEMOVAR and FOAM-AC. The systems assimilate in situ and satellite SST observations, in situ temperature and salinity profile observations, altimeter SLA data and satellite sea ice concentration data. The satellite SST data is subsampled level 2 data from GHRSST and includes data from the Advanced Microwave Scanning Radiometer Earth observing system (AMSR-E), the Advanced Along-Track Scanning Radiometer (AATSR), the Advanced Very High Resolution Radiometer (AVHRR) on board NOAA and MetOp satellites. The main source of temperature and salinity profile observations is the network of about 3000 Argo floats, but profile data is also obtained from expendable bathythermograph (XBT), moored buoy arrays and CTDs. The altimeter data is from CLS/AVISO and is provided by 3 instruments: Jason-1, Jason-2 and Envisat. The Sea ice data is provided by EUMETSAT OSI-SAF and is data from a Special Sensor Microwave/Imager (SSMI).

The FOAM-NEMOVAR re-analysis was run for a 3 year period between January 2008 and December 2010. A three month spin up was also included prior to this. After the first 5 months the re-analysis was stopped and some final developments and tuning were included in the system, the finalised configuration therefore ran from the 8th of June 2008. The period used for validation in this study is between 8th June 2008 and the 7th of June 2009. This was chosen because of the availability of a FOAM-AC re-analysis (which was run between January 2007 and August 2009).

© Crown Copyright 2013

Table 2: Summary of differences in the FOAM-AC and FOAM-NEMOVAR configurations

	FOAM-AC	**FOAM-NEMOVAR**
Assimilation scheme	AC	NEMOVAR
Sea ice model	Lim2: 1 thickness category and zero-layer thermodynamics	CICE: 5 thickness catergories and zero-layer thermodynamics
Model configuration	ORCA025 1/4 degree global configuration with 50 vertical levels	ORCA025L75 1/4 degree global configuration with 75 vertical levels
Haney forcing	Haney retroaction term on SST	Haney retroaction term on SST and SSS
Diagnostic output	bespoke diafoam diagnostics	iomput diagnostics
Newtonian damping	no Newtonian damping	Newtonian damping of 3D T and S fields to 1/4 Degree climatologies with timescale of one year
Horizontal viscosity	mixed laplacian and bilaplacian	bilaplacian
Penetrating solar radiation	UM Band 1 flux and 2-band scheme for vertical distribution	UM total SW flux and RGB scheme for vertical distribution with uniform Chlorophyll value
TKE scheme	New version of TKE scheme. $rn_{lmin} = rn_{lmin0} = 0.4$	New version of TKE scheme. $rn_{lmin} = 0.001$, $rn_{lmin0} = 0.01$
Bottom friction	no geographical variation of parameters	geographical variation of parameters included: enhanced mixing in Indonesian Throughflow, Denmark Strait and Bab al Mandeb (Red Sea)
Bottom boundary layer scheme	none	advective and diffusive bottom boundary layer for T and S
Tidal mixing parameterisation	no tidal mixing	tidal mixing included: K1 and M2 mixing climatologies
Enhanced mixing at river mouths	enhanced mixing of $1.5e^{-3}m^2/s$ over top 25m	enhanced mixing of $2.0e^{-3}m^2/s$ over top 10m
Initial conditions	from operational system	from a NOC 40 year free model run
SST bias	Bug: GHRSST bias fields were not applied to all satellite SST types	bug fixed

6 Ice Assimilation

The ice model used in FOAM-NEMOVAR is CICE, a multi-category EVP sea ice model (Hunke and Lipscomb [2010]). In the runs described here there are five ice categories and a snow category. Each category has an ice area (as a fraction of the grid cell) and ice volume associated with it. The total ice area (or ice concentration) in a grid cell is obtained adding up all the ice area for all categories. This will always be between 0 and 1.

If the ice concentration increment provided by the assimilation is positive this is introduced to the model by adding additional ice with a specified thickness of 50 cm to the first ice category only. If the ice concentration increment is negative the ice is first removed from the lowest category and then,

© Crown Copyright 2013

if needed, it is removed from progressively higher categories until the required ice concentration increment is achieved. Regardless of whether ice concentration is increased or decreased the prior snow depth is maintained. The scheme includes salt and fresh water balancing but this is not applied to the ocean currently. Future work will reintroduce this.

7 Bias Correction

7.1 SST Bias Correction system

As with most data assimilation systems, NEMOVAR implicitly assumes that all observations are unbiased. Unfortunately SST data produced by satellite instruments are prone to bias due to errors in the specified non-constant atmospheric constituents, especially water vapor and aerosols (Emery et al. [1994]), attenuating emitted thermal radiation before it reaches the satellite sensor. Consequently, a bias correction scheme has been developed to remove biases from satellite observations before they are passed to NEMOVAR.

The bias correction scheme is similar in operation to the scheme employed in FOAM-AC (Martin et al. [2007] and Donlon et al. [2011]). The methodology proceeds by correcting the data towards a reference set of observations that are assumed unbiased. At the beginning of the routine matchups are found between the observations to be corrected and the reference data. The matchups correspond to observations that occur within one day of each other and are separated by less than 25 km on a great circle. Once the matchups are found they are used in the calculation of observation differences where reference observations are subtracted from biased observations. These differences are then treated as "observations of bias" and are assimilated using NEMOVAR into a pre-existing background field of bias. There are a number of differences between this SST bias correction application of NEMOVAR and how NEMOVAR is applied within the data assimilation step:

- NEMOVAR is setup in a 2-dimensional configuration with a single vertical level; this is because the bias field is a 2-dimensional quantity confined to the ocean surface.
- There is no model for advancing the bias fields through time, instead the background bias field is given by the bias analysis of the previous day relaxed towards zero with an e-folding timescale of 10 days.
- Because the bias is believed to be primarily caused by atmospheric effects, a continent mask is not applied during the assimilation. As a result the bias analysis field covers the whole domain without interruption. Biases therefore spread across land boundaries.
- In line with the old FOAM SST bias correction system, the bias is assumed to have a long 7° lengthscale.
- Observation errors are the same as for SST assimilation in NEMOVAR.

© Crown Copyright 2013

- The background error is set to a constant 0.1 K everywhere. This is chosen to be comparable with the FOAM-AC settings.

After it is calculated the analysis bias field is subtracted from the observations according to

$$y_n = \bar{y}_n - b, \tag{12}$$

where y_n is the n^{th} unbiased observation, $\bar{y}_n$ is the n^{th} biased observation, and b is the bias field at the location of observation n. The unbiased observations are then used in the data assimilation step in FOAM. The SST bias correction step is an extra operation in the FOAM cycle and is performed prior to the observation operator step.

For the global analysis system described in this text we bias correct observations from NOAA-AVHRR, AMSR-E, and MetOp-AVHRR (see Section 5 for a description of the observations). All of these instruments are individually bias corrected towards in-situ data and towards data from the AATSR sensor. Unlike data from the other satellite instruments, data from AATSR is assumed unbiased because of its on-board black body calibration system and duel view optics.

To illustrate the biases calculated by the SST bias correction scheme, Figure 12 shows the bias correction field for SST observations from the AMSR-E instrument on the last day of our model hindcast. In this case the biases are mostly positive, but they do vary throughout the model run. (An interesting feature of the plot is the long lengthscales that are apparent; these result from the 7° correlation lengths used by NEMOVAR in calculating the bias field).

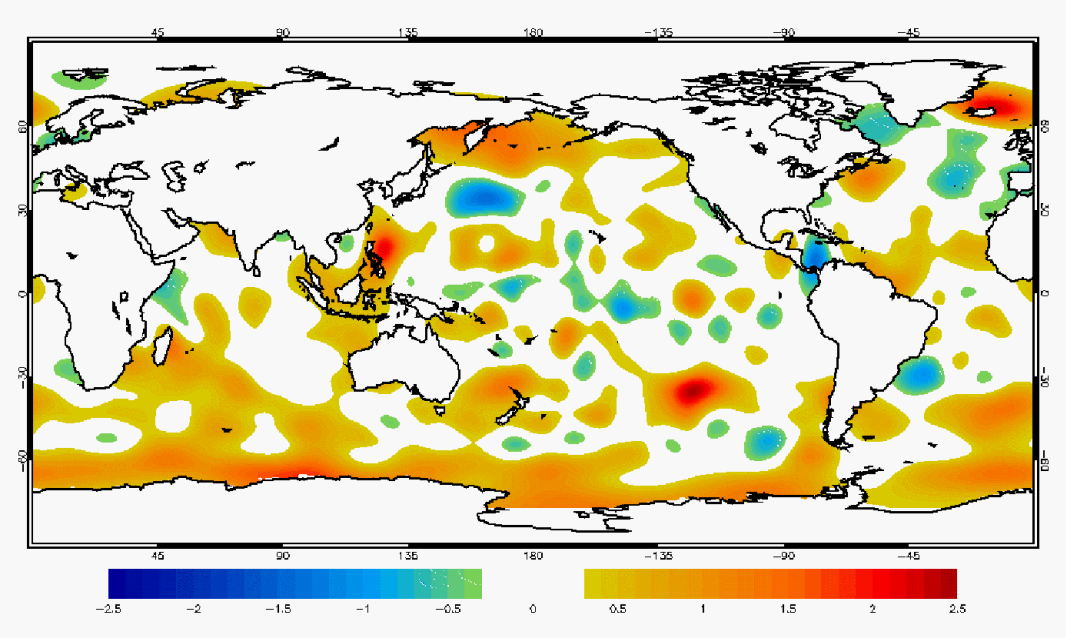

Figure 12: Bias correction field for AMSR-E SSTs on the 31$^{\text{st}}$ December 2010. For clarity, bias fields over land are not shown.

© Crown Copyright 2013

7.2 Altimeter Bias Correction system

Ocean altimeter data have provided routine sea-level or dynamic topography information which is crucial for observing the ocean circulation on the mesoscale. However, altimetry can only measure the sea level anomaly (SLA) because the absolute dynamic topography (ADT) is the sea level with respect to the gravity geopotential surface (the geoid) which is not sufficiently well known for oceanographic purposes. When assimilating satellite data into ocean circulation models, it is necessary to add a mean dynamic topography (MDT) to the altimeter measurements of the SLA. In the case of FOAM this is the CNES-CLS09 MDT (Rio et al. [2011]) which is a combination of GRACE (Gravity Recovery And Climate Experiment) satellite gravity measurements and estimates of the MDT based on drifter and other in-situ data.

All MDTs can have errors that may be much larger than that of the altimeter data, although these are constant in time so can be treated as a bias to the observations. This bias can be estimated as part of the data assimilation procedure using the method of observation bias correction described in Lea et al. [2008]. This method is used in the FOAM-AC system. Here we describe the work to adapt this method to NEMOVAR.

The method requires the addition of an altimeter bias field $\mathbf{b}$ to the data assimilation control vector and to the 3D-Var incremental cost function as follows

$$\begin{aligned} 2J(\delta\mathbf{x},\mathbf{b}) &= (\delta\mathbf{x})\mathbf{B}^{-1}(\delta\mathbf{x}) + (\mathbf{b}^o-\mathbf{b})^T\mathbf{T}^{-1}(\mathbf{b}^o-\mathbf{b}) + (\mathbf{b}-\mathbf{b}^f)^T\mathbf{O}^{-1}(\mathbf{b}-\mathbf{b}^f) \\ &+ (\mathbf{d}-\mathbf{H}_{\text{alt}}\delta\mathbf{b}-\mathbf{H}\delta\mathbf{x})^{\mathbf{T}}\mathbf{R}^{-1}(\mathbf{d}-\mathbf{H}_{\text{alt}}\delta\mathbf{b}-\mathbf{H}\delta\mathbf{x}) \end{aligned} \quad (13)$$

where $\mathbf{b}^o$ is the initial bias, usually set to zero. The bias estimated from the previous analysis $\mathbf{b}^f$ is assumed to remain constant. The altimeter observations are bias corrected by subtracting the interpolated bias field using the altimeter observation operator $\mathbf{H}_{\text{alt}}$.

In order to implement this method we must provide estimates of the error covariances. Currently we use the errors provided with the CLS-CNES09 MDT. The errors are inflated by a factor of 5 to more closely represent the known variability between MDT products as in Lea et al. [2008]. This gives us the standard deviations of the error covariance $\mathbf{T}$ which controls the size of overall bias. As with the model control variables the covariances for the bias are modelled using a diffusion operator generating a correlation lengthscale of 40 km. The error covariance $\mathbf{O}$ controls the size of the increments made to the bias each day. This is assumed to be $0.01\mathbf{T}$ so that the bias builds up gradually with time. Currently the overall bias constraint is not implemented in the cost function (and it is not immediately obvious how to do so in an incremental scheme). It may be most convenient to add a relaxation to the bias between analysis steps which prevents it from moving outside the range specified by the error covariance $\mathbf{O}$.

For the initial implementation, the cost function actually implemented is

© Crown Copyright 2013

$$
\begin{aligned}
2J(\delta\mathbf{x},\mathbf{b}) &= (\delta\mathbf{x})\mathbf{B}^{-1}(\delta\mathbf{x}) + (\mathbf{b}-\mathbf{b}^{f})^{T}\mathbf{O}^{-1}(\mathbf{b}-\mathbf{b}^{\mathbf{f}}) \\
&+ (\mathbf{d}-\mathbf{H_{alt}}\delta\mathbf{b}-\mathbf{H}\delta\mathbf{x})^{\mathbf{T}}\mathbf{R}^{-1}(\mathbf{d}-\mathbf{H_{alt}}\delta\mathbf{b}-\mathbf{H}\delta\mathbf{x}) \qquad (14)
\end{aligned}
$$

The method is shown to work as well as the scheme running in the FOAM-AC scheme (which did have the overall bias constraint). Typically the global RMS observation minus background error is reduced by 2cm when the altimeter bias correction scheme is used. There are also signs that there are beneficial impacts on the fit to temperature and salinity data indicating that the bias corrected altimeter data is more consistent with profile data.

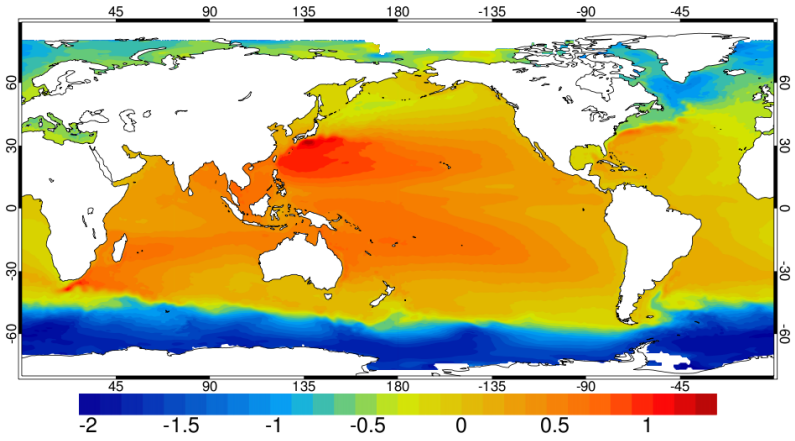

Figure 13: The CLS-CNES09 MDT in m.

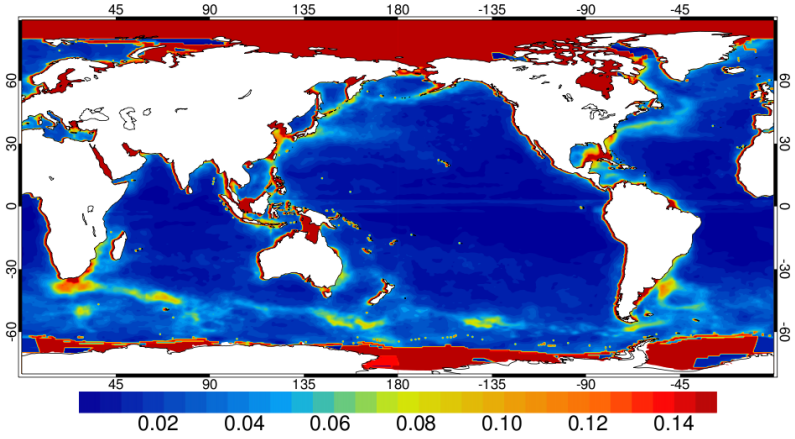

Figure 14: The bias error standard deviation field in m provided with CLS-CNES09 MDT.

In future we plan to use an entirely gravity based MDT derived from GRACE and GOCE (Gravity field and steady-state Ocean Circulation Explorer) satellites. The errors on this are rather different to the CLS-CNES09 MDT and typically large on shorter length-scales. A scheme has been developed

© Crown Copyright 2013

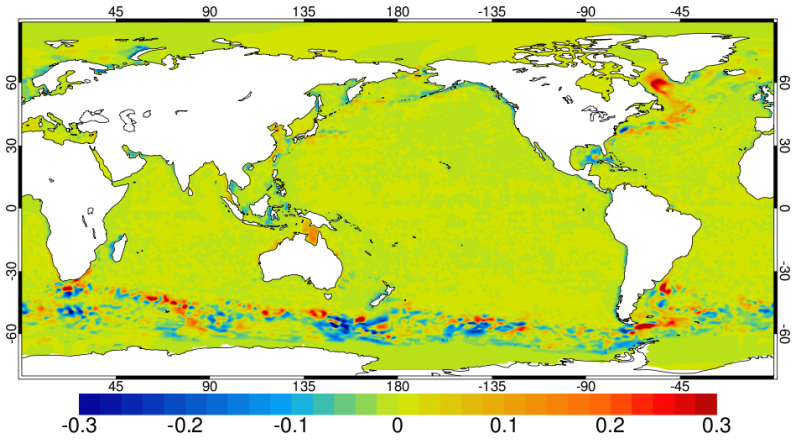

Figure 15: The bias field calculated in a NEMOVAR hindcast on 31 Dec 2009 in m

whereby the bias is filtered using the diffusion operator to remove the large scales leaving only the shorter lengthscales to be applied to the observation bias. This filtered bias is not used in the experiments described in this report.

© Crown Copyright 2013

8 Re-Analysis Results

The results from the FOAM-NEMOVAR re-analysis are presented below. The majority of the results are from the observation minus background statistics. For temperature, salinity, SSH and sea-ice the statistics are calculated from the observation-background differences generated in the observation operator step. The observation minus background statistics calculated from surface drifter velocity data are also shown. Since velocities are not assimilated in FOAM-NEMOVAR (or FOAM-AC) the surface drifter velocities provide an independent data source for comparison and are calculated using the technique of Blockley et al. [2012]. The statistics from FOAM-NEMOVAR and FOAM-AC are compared to assess the performance of FOAM-NEMOVAR. Some surface field plots are also presented to illustrate differences between FOAM-NEMOVAR and FOAM-AC.

8.1 Observation minus Background statistics

SST

In this section the background SSTs are validated against in-situ SST observations. The root mean square error (RMSE) and mean difference between the observations and background are shown in Figure 16. From Figure 16 there is a significant reduction in the RMSE in the FOAM-NEMOVAR run. The overall RMSE error is reduced by 28% from 0.649^oC in FOAM-AC to 0.468^oC in FOAM-NEMOVAR. There is also a large reduction in the mean error, with the FOAM-AC mean error -0.093^oC and the FOAM-NEMOVAR mean error -0.039^oC. Some of this improvement may be due to the new variational system and the specification of the errors in FOAM-NEMOVAR, but the bug fix to the SST bias (discussed in Table 2), is also assumed to an impact on the results. However, the SST RMSE for FOAM-NEMOVAR is encouragingly low and comparable to results from OSTIA (Stark et al. [2007]). There is an increase in the RMSE at the end of the period in both FOAM-NEMOVAR and FOAM-AC, the reason for this will be discussed later.

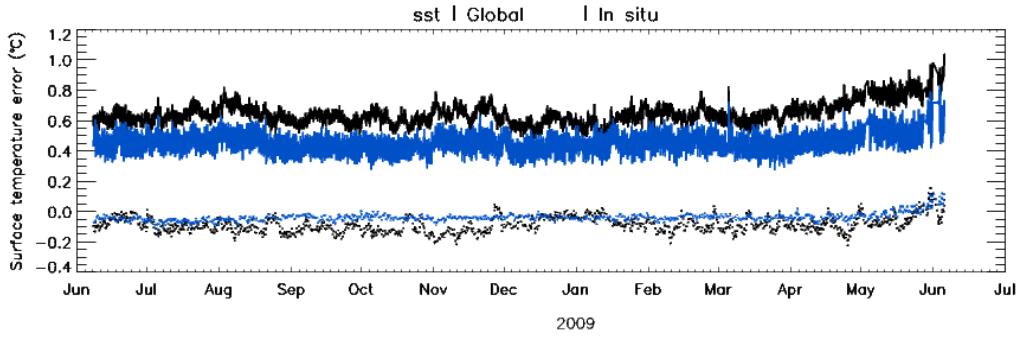

Figure 16: In-situ SST observations minus background statistics. The blue line is from FOAM-NEMOVAR and the black line is from FOAM-AC. The solid line is RMSE and the dashed line is mean error.

© Crown Copyright 2013

SSH

Figure 17 shows the observation minus background statistics for SSH. It is difficult to see any obvious improvements in FOAM-NEMOVAR in Figure 17. However, if we consider the overall statistics, FOAM-NEMOVAR has an RMSE of $8.3cm$ while FOAM-AC has an RMSE of $8.6cm$, so there is a small improvement in the RMSE in FOAM-NEMOVAR. The RMSE for FOAM-NEMOVAR in Figure 17 appears to still be improving at the beginning of the validation period. It is therefore possible that if we validated FOAM-NEMOVAR for a later period that the RMSE error will have improved further.

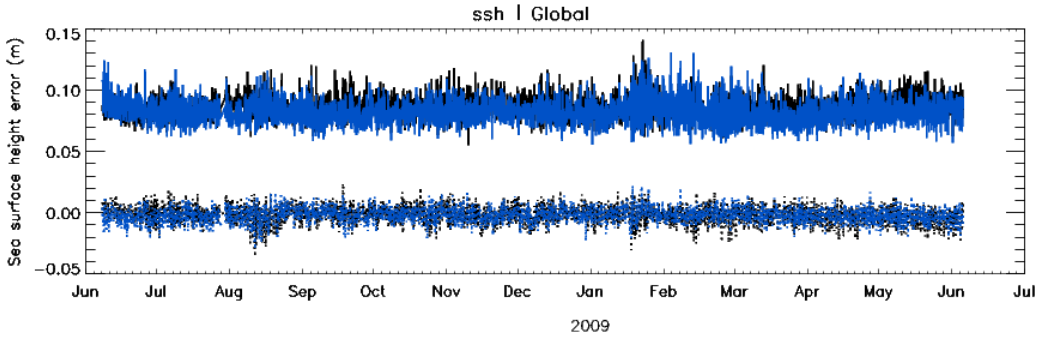

Figure 17: Observed SSH minus background statistics. The plot has the same format as Figure 16.

Sea Ice Concentration

Figure 18 shows a significant improvement in the sea ice concentration in FOAM-NEMOVAR. This is particularly noticeable at the end of the validation period where the RMSE results are very poor in FOAM-AC. Further investigation of this period showed that the poor results are related to corrupt wind forcing fields between April and July 2009. The same forcings are used for FOAM-NEMOVAR, but the sea-ice concentration statistics remain more stable in FOAM-NEMOVAR during this period. This could be because the data assimilation in NEMOVAR is better constraining the model, or it could be related to using different sea ice models in the two systems. This corruption of the forcings also explains the poorer results in the SST statistics at the end of the validation period.
Ignoring this period of corruption, we still see a good improvement in the sea-ice concentration RMSE. This may in part be due to changes in the data assimilation, but the change in sea ice model is likely to have had an impact.

Temperature Profiles

Table 3 shows observation minus background statistics for temperature profiles. The global statistics suggest an overall improvement in the RMSE in FOAM-NEMOVAR. This improvement is also seen at the majority of regional locations, the exception being the Tropical and South Pacific. However, if we consider the plots of statistics over depth in Figure 19 the results for FOAM-NEMOVAR are less positive. In the global plot there is a clear and significant improvement in the FOAM-NEMOVAR

© Crown Copyright 2013

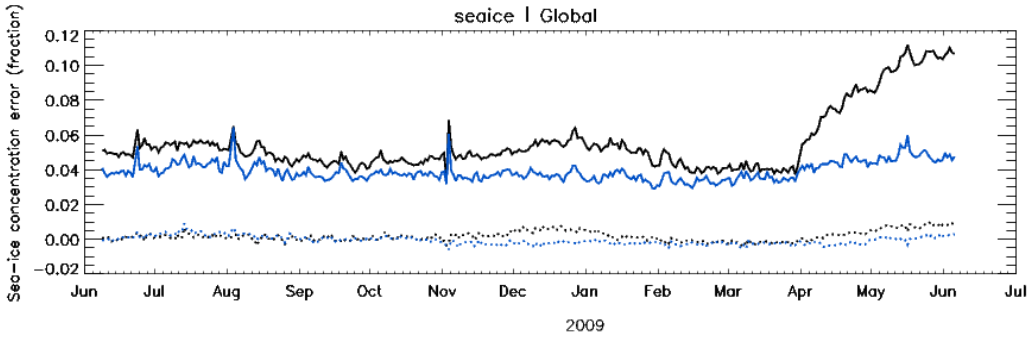

Figure 18: A plot of observed sea ice concentration minus background sea ice concentration statistics.The plot has the same format as Figure 16.

RMSE at the surface and to depths of around 50m, but between 100m and 400m the FOAM-NEMOVAR RMSE is larger than the FOAM-AC RMSE. The total global statistics in Table 3 show better results in FOAM-NEMOVAR because the surface statistics have more weight than statistics at depth due to a larger number of observations at the surface. Profile plots of the statistics in the North Pacific and South Atlantic are also presented in Figure 19. The plots show two contrasting cases. In the South Atlantic there is actually a reduction in the FOAM-NEMOVAR RMSE at all depths, where as the North Pacific results are more consistent with the global case. From the plots it is also noticeable that there are larger biases in FOAM-NEMOVAR. For the global and North Pacific case there is a large mean error in FOAM-NEMOVAR between 100m and 400m. This bias dominates the difference in the RMSE between FOAM-NEMOVAR and FOAM-AC.

Both the shorter background error correlation lengthscales and changes to the model parameterisations could be impacting on the bias in FOAM-NEMOVAR. Since there are fewer observations at depth, the shorter correlation lengthscales may make it difficult for the assimilation to constrain any model biases below the surface. Changes in NEMO to the mixing parameterisations, Haney forcing and Newtonian damping could also be increasing model bias in the temperature and salinity profiles. All these areas should be investigated in future work.

Table 3: Temperature profile Observation minus background errors

Region	FOAM-AC RMSE(mean error)	FOAM-NEMOVAR RMSE(mean error)
Global	0.674 (-0.007)	0.664 (-0.016)
North Atlantic	0.892 (-0.029)	0.859 (-0.019)
Tropical Atlantic	0.614 (0.000)	0.603 (0.018)
South Atlantic	0.825 (-0.025)	0.726 (0.008)
North Pacific	0.714 (-0.015)	0.711 (-0.027)
Tropical Pacific	0.451 (0.007)	0.510 (0.012)
South Pacific	0.481 (0.001)	0.497 (-0.022)
Indian Ocean	0.571 (0.002)	0.570 (-0.023)
Southern Ocean	0.700 (-0.011)	0.634 (-0.019)

© Crown Copyright 2013

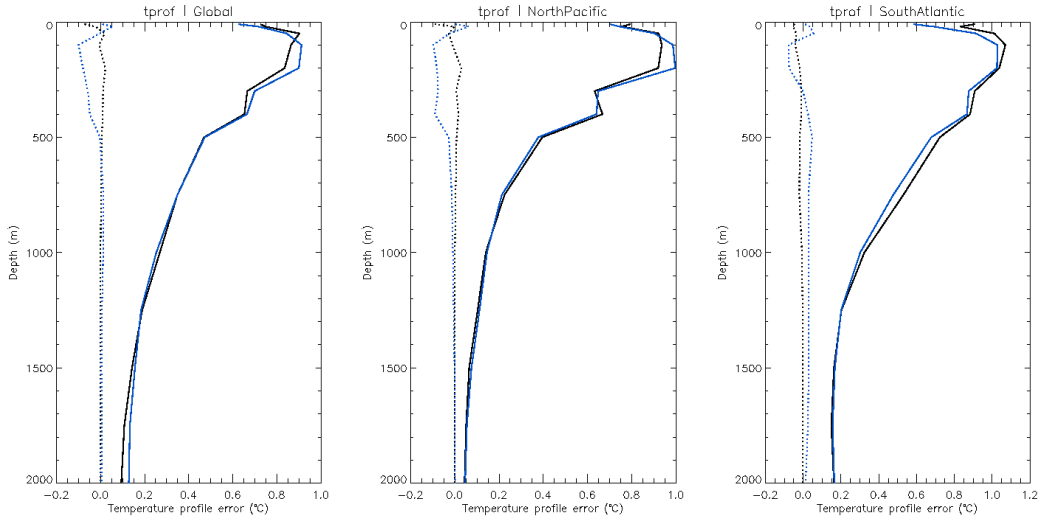

Figure 19: Observed temperature minus background profile statistics. The plot has the same format as Figure 16. Left hand plot shows the global statistics, centre plot shows the North Pacific statistics and right hand plot shows the South Atlantic statistics.

Salinity Profiles

The statistics for the salinity profiles are shown in Figure 20. FOAM-NEMOVAR produces a degradation of the salinity results. In the plot of global statistics the FOAM-NEMOVAR has a larger RMSE and mean than FOAM-AC in the top 300m of the water column. A similar pattern is seen in the regional results. The North Pacific is an example of a region where the difference in the FOAM-NEMOVAR and FOAM-AC errors is relatively small. In the South Atlantic there is a significant degradation in the statistics in FOAM-NEMOVAR. There is a large increase in the RMSE above 300m and this is dominated by the large difference in the mean error. Interestingly the pattern of very bad results in the South Atlantic and less poor results in the North Pacific contrasts with the results for the temperature profiles. This may imply that process which are improving temperature in some areas are also leading to the degradation of salinity. The altimeter assimilation also appears to impact negatively on the salinity results and this will be discussed in more detail in section 9.2.

Surface Currents

The velocities are validated against independent surface drifter data using the technique of Blockley et al. [2012]. Figure 21 shows the RMSE and mean error for the South Atlantic. There is a reduction in the RMSE in FOAM-NEMOVAR compared to FOAM-AC for both the meridional and zonal currents. Figure 22 shows the statistics for the Tropical Pacific. In this region the RMSE increases in FOAM-NEMOVAR. This was a general trend in the velocities, with FOAM-NEMOVAR producing better results than FOAM-AC in the extratropics but worse results in the tropics. One possibility is that background error lengthscales used for assimilating temperature and salinity are too long in the tropics. This assumption will be investigated further in section 9.1.

© Crown Copyright 2013

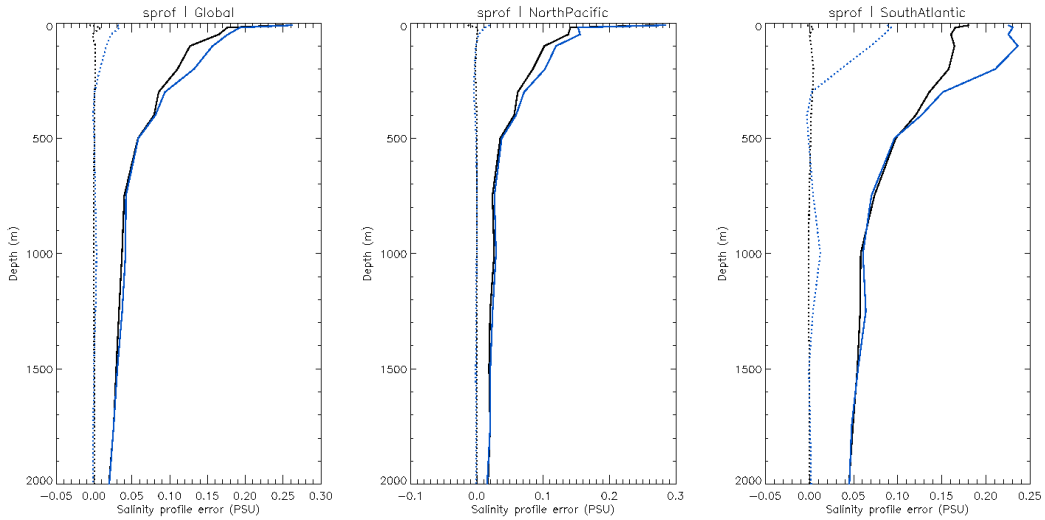

Figure 20: Observed salinity minus background profile statistics. The plot has the same format as Figure 19.

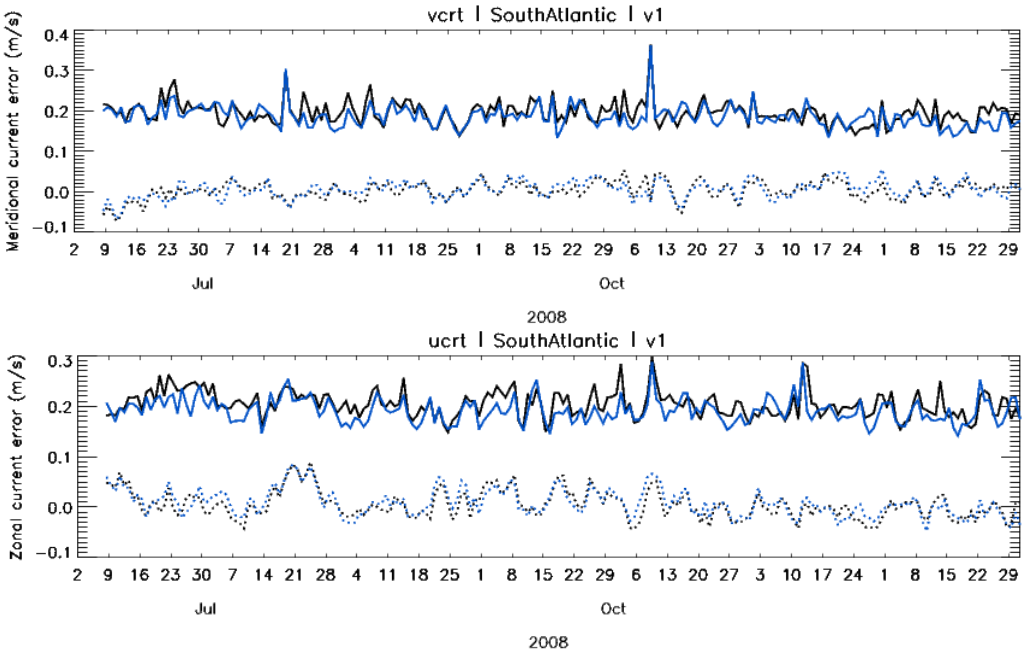

Figure 21: Observed velocity minus background statistics for the South Atlantic. The plot has the same format as Figure 16. Top plot is the meridional currents, bottom plot is the zonal currents.

© Crown Copyright 2013

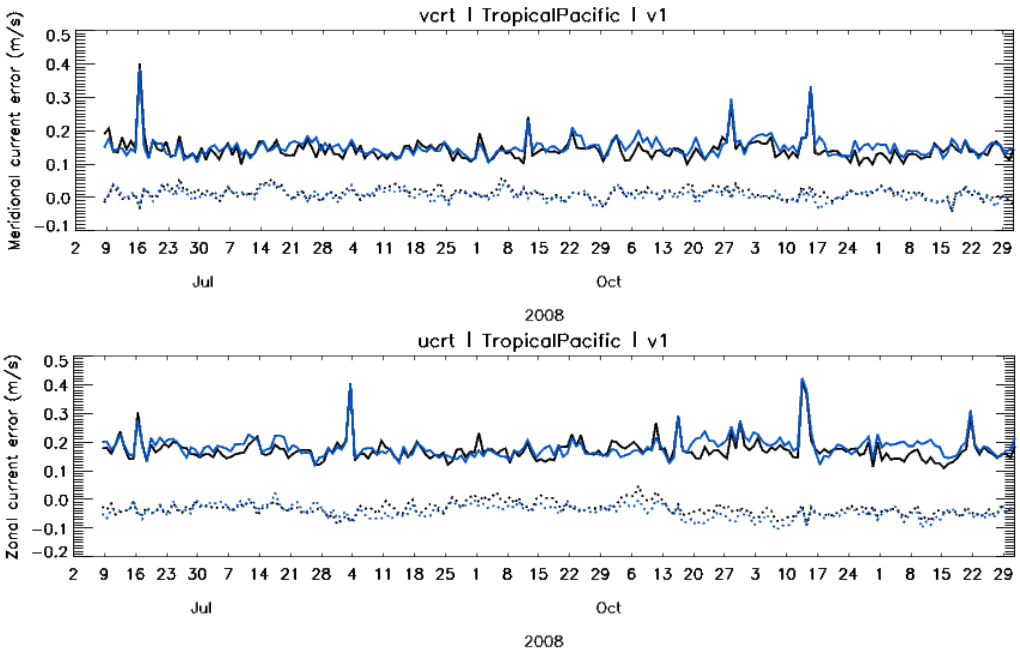

Figure 22: Observed velocity minus background statistics for the Tropical Pacific. The plot has the same format as Figure 21.

© Crown Copyright 2013

8.2 Comparisons of SSH fields

Figures 23, 24 and 25 show plots of SSH fields from FOAM-AC and FOAM-NEMOVAR in different regions. In Figure 23 the fields are quite similar. FOAM-NEMOVAR produces a more defined Gulf-stream front while there is more eddy shedding along the front in FOAM-AC. FOAM-NEMOVAR is also possibly resolving more of the high resolution features. This could be because data is being better fitted in FOAM-NEMOVAR or related to the shorter horizontal correlation lengthscale in FOAM-NEMOVAR compared to FOAM-AC. Figure 24 shows similar results in the region of the Kuroshio current with a more defined front in FOAM-NEMOVAR and a smoother field in FOAM-AC. The results for the Indian Ocean shown in Figure 25 are generally consistent between FOAM-NEMOVAR and FOAM-AC. There is, however, some increased eddy activity in the Bay of Bengal and in the Mozambique Channel in FOAM-NEMOVAR compared to FOAM-AC.

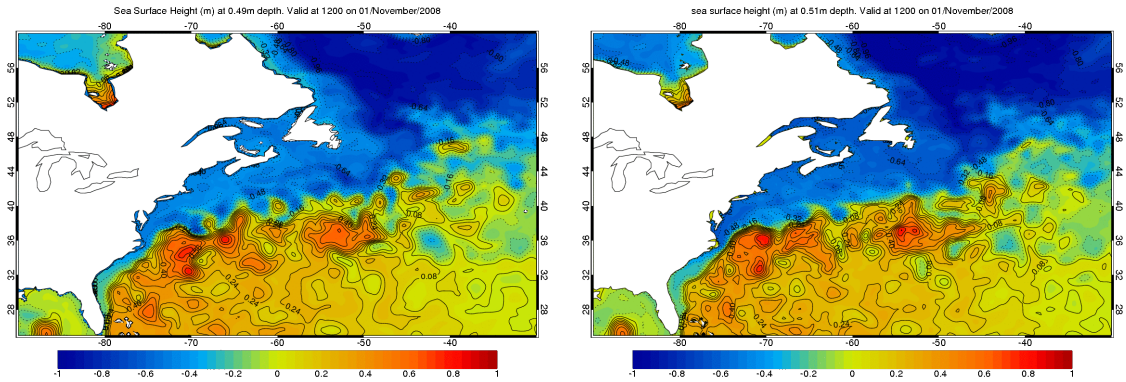

Figure 23: Plots of daily mean SSH fields in the Gulf Stream region for 01/11/2008. The left hand plot is from FOAM-AC, the right hand plot is from FOAM-NEMOVAR.

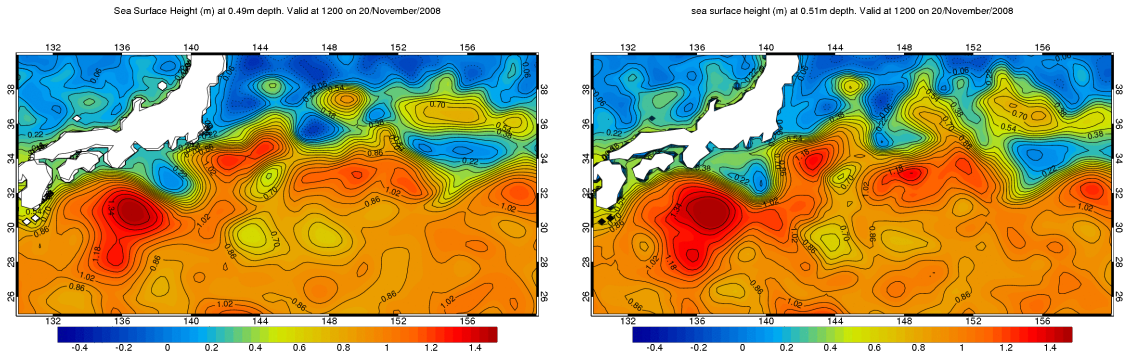

Figure 24: Plots of daily mean SSH fields in the Kuroshio current region for 20/11/2008. The left hand plot is from FOAM-AC, the right hand plot is from FOAM-NEMOVAR.

© Crown Copyright 2013

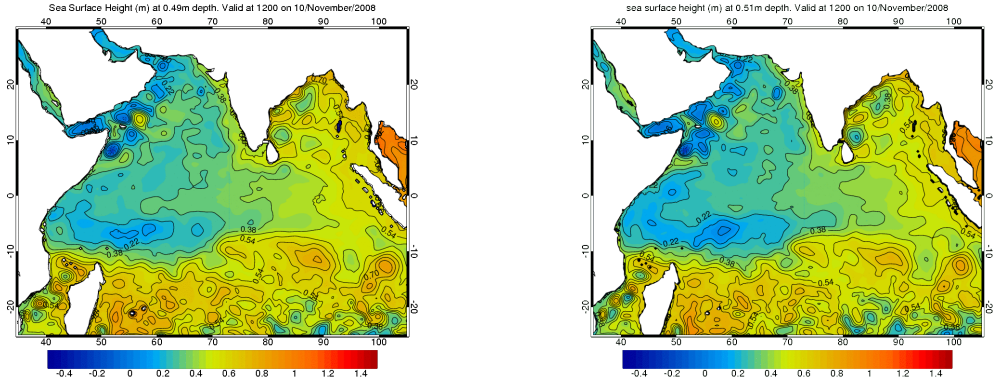

Figure 25: Plots of daily mean SSH fields in the Indian Ocean for 10/11/2008. The left hand plot is from FOAM-AC, the right hand plot is from FOAM-NEMOVAR.

8.3 Comparisons against OSTIA

In this section, fields of SST from FOAM-NEMOVAR and FOAM-AC are compared to outputs from the SST analysis product, OSTIA (Donlon et al. [2011]). Figure 26 shows the SST fields in the Gulf Stream. FOAM-NEMOVAR and FOAM-AC both produce SSTs which have more small scale variability than OSTIA. OSTIA is known to produce overly smooth fields (Reynolds et al. [2013]) so we expect to see more variability in the model outputs. The SST results for FOAM-NEMOVAR are very positive. We see a good correlation in the dominant features between FOAM-NEMOVAR and OSTIA. This can be seen particularly along the edge of the front. In comparison, the results for FOAM-AC are poorer with fewer comparable features identifiable. Similar results are seen along the Kuroshio current in Figure 27. The features along the front are very consistent between FOAM-NEMOVAR and OSTIA but are quite different in FOAM-AC. Some of this improvement to the SSTs may be related to changes in the data assimilation. The shorter background error correlation length-scales for temperature may have improved the results and it is reassuring to find that using shorter correlation lengthscales has not made the temperature fields noisy. The improvements could also be related to changes to the model parameterisations.

8.4 Summary of the results

The results from this study show that there are generally improvements in the surface fields for FOAM-NEMOVAR compared to FOAM-AC. However, the profile results are more mixed with some degradation in the temperature and salinity statistics in the top 50-500m of the water column. There are various differences between the FOAM-NEMOVAR and FOAM-AC configurations and this makes it difficult to attribute any improvements or degradations to any specific change. Future work will focus on producing runs which allow for a cleaner comparison between the two data assimilation systems.

© Crown Copyright 2013

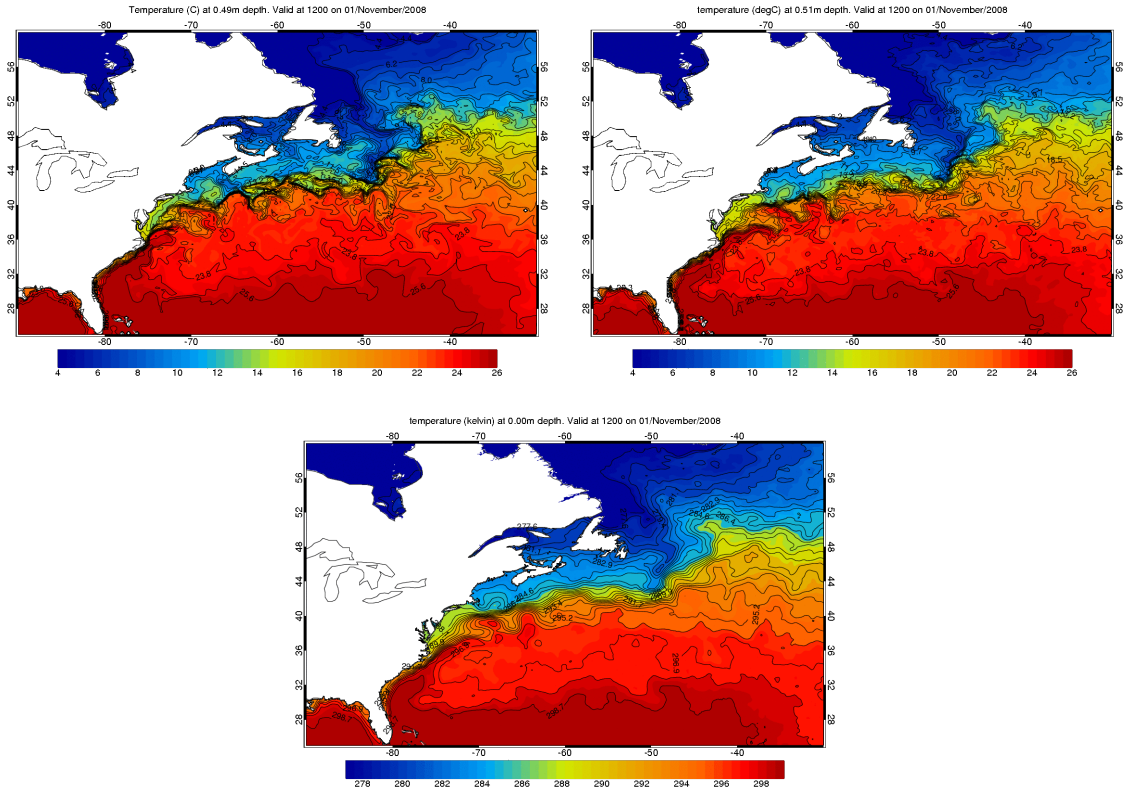

Figure 26: Plots of daily mean SST fields in the Gulf Stream region for 01/11/2008. The top left hand plot is from FOAM-AC, the top right hand plot is from FOAM-NEMOVAR, the bottom plot is from OSTIA.

© Crown Copyright 2013

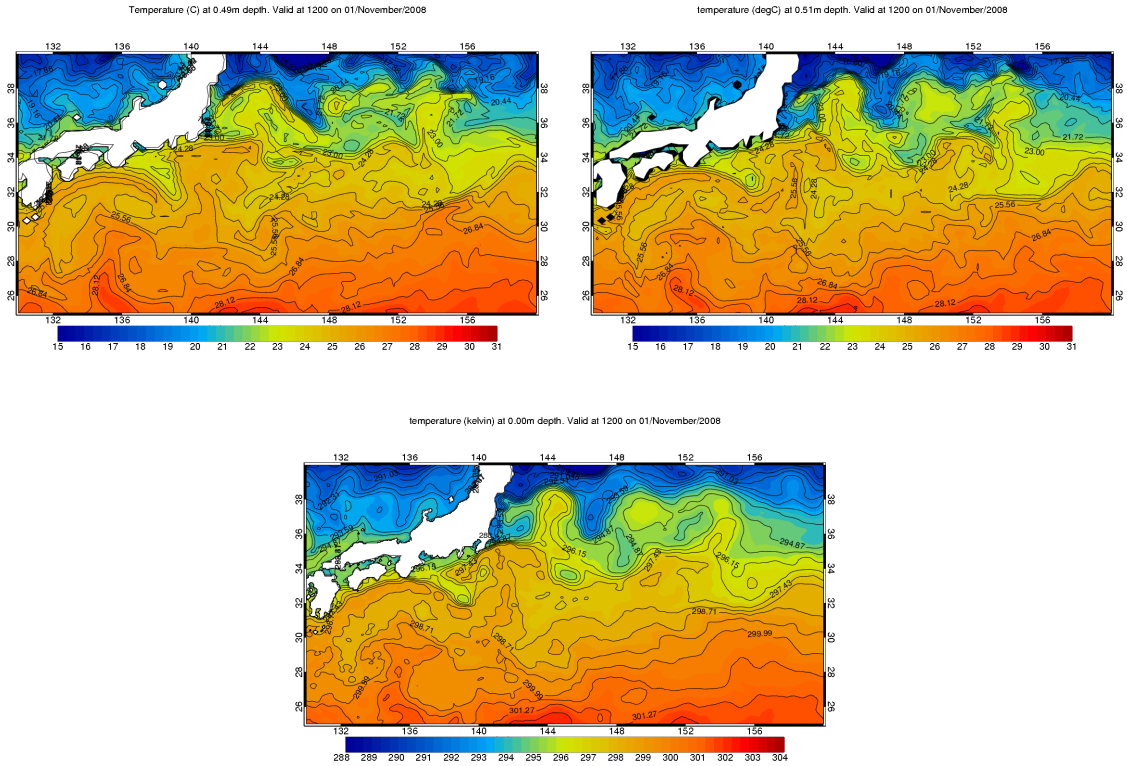

Figure 27: Plots of daily mean SST fields in the Kuroshio current region for 01/11/2008. The top left hand plot is from FOAM-AC, the top right hand plot is from FOAM-NEMOVAR, the bottom plot is from OSTIA

© Crown Copyright 2013

9 Further developments for FOAM-NEMOVAR

In this section further changes and developments for the NEMOVAR system are described. These were not included in the FOAM-NEMOVAR trial presented above but have subsequently been implemented in the Met Office system. These include changes to the background error correlation lengthscales in order to improve tropical currents, changes to the background salinity error and changes to the profile data set to eliminate bad profile observations.
An additional change is a bug fix for the TKE mixing scheme. Any future runs will include this bug fix.

9.1 Equatorial background error correlation lengthscales

The correlation length scales in the FOAM-NEMOVAR hindcast were set to match the Rossby radius in the north-south and east-west directions (see section 4.2). Near the equator the Rossby radius tends to infinity and therefore a maximum cap is applied. It is often observed that features in the equatorial region are correlated over longer lengthscales zonally than meridionally. So in the initial runs with NEMOVAR the maximum length scale was capped at 300 km zonally and 150 km meridionally.
Comparison of the FOAM-NEMOVAR currents with those from surface drifters (using the method of Blockley et al. [2012]) showed a degraded fit to currents in the equatorial regions (section 8.1). One notable difference between FOAM-AC and FOAM-NEMOVAR is its specification of the horizontal lengthscales. In the FOAM-AC scheme the lengthscales were 40 km for the mesoscale component and 400 km for the synoptic scale and there was no anisotropy at any latitude. This motivated doing some more investigation of the lengthscales used in NEMOVAR.
The Quick Canadian method (Polavarapu et al. [2005]) was used to produce error estimates from a one year model run. The correlation of the 1 day model field differences with the field difference at a specified point in the equatorial region shows that these differences near the equator have a lengthscale of around 150km meridionally and a similar, perhaps slightly longer, lengthscale zonally. There is more evidence of anisotropy in sea surface height than sea surface temperature (see examples in Figure 28). Away from the equator there are often quite large scale correlations perhaps because atmospheric forcing variability is dominant in these regions. This supports the old two scales approach and there is work planned to implement this in future versions of NEMOVAR. In many locations particularly near coastlines the correlations are notably anisotropic, but representing this in NEMOVAR is not possible with the existing parametrizations. Given this information we performed a 3 month test run which retains the Rossby radius lengthscale but sets the maximum to 150 km in both the East-West and North-South directions.

The test involves a 3 month run starting on 1 July 2008. This can be compared with a NEMOVAR run using the old lengthscales and the FOAM-AC hindcast. The results of the assessment of the fit to drifter currents in the Tropical Pacific are summarised in Table 4. Although the differences are

© Crown Copyright 2013

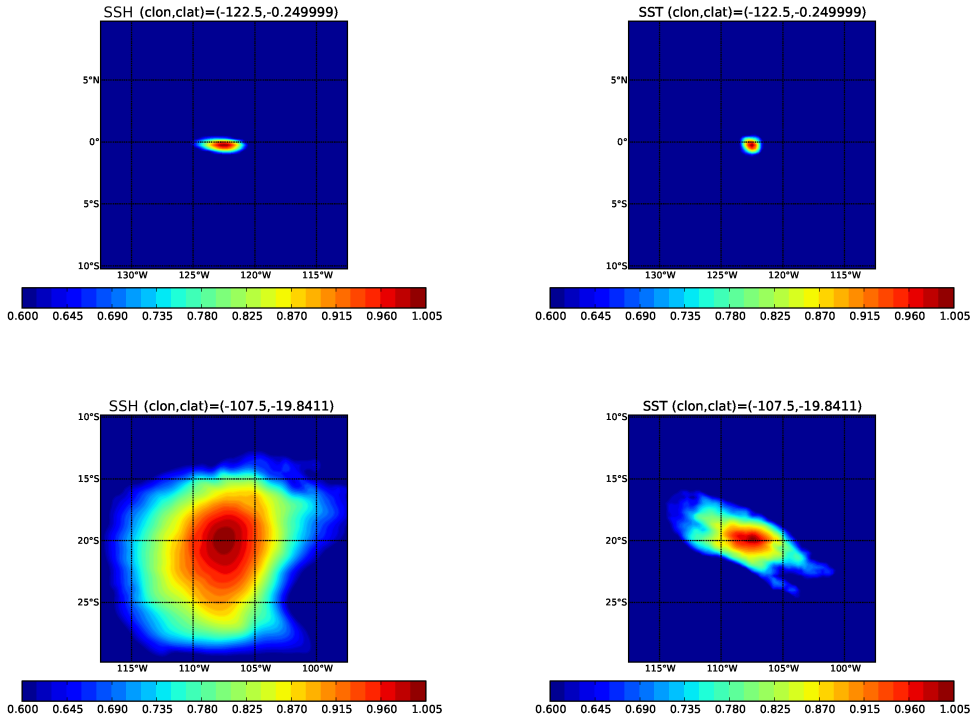

Figure 28: The correlations at 2 points with the surrounding model grid points in SSH and SST

subtle there does appear to be a marginal improvement in the correlation and RMS drifter errors. The assessment of this is complicated by other differences between the NEMOVAR old lengthscale run including a new salinity background error parametrization which may have slightly reduced the fit to altimeter data. Therefore, we decided to implement the 150 km maximum lengthscales for future runs.

Table 4: Velocity Statistics in the Tropical Pacific.

	FOAM-AC	NEMOVAR old lsc	NEMOVAR new lsc
zonal velocity RMS	0.175	0.181	0.179
meridional velocity RMS	0.148	0.149	0.150
zonal velocity correlation	0.758	0.743	0.749
meridional velocity correlation	0.538	0.542	0.540

9.2 SSH balance and salinity

A particular problem with the FOAM-NEMOVAR hindcast is that the salinity (obs minus background) error statistics are found to be noticeably worse than those in the FOAM-AC system. This problem largely went away when we turned off altimeter assimilation in a test run.

Investigation of the problem identified the South Atlantic as a region where there was a particular issue with assimilating altimeter data. We therefore focus on a single observation test at the

© Crown Copyright 2013

location 45.59W 39.55S. It is important to point out that SSH information is propagated into temperature and salinity via the adjoint of the balance operator. Therefore the structure of the balance operator and also the background errors of the variables are critical to how the SSH information is converted into density increments, and thence into temperature, balanced and unbalanced salinity increments. This particular single observation generates very large salinity increments at about 200 m depth, exactly where the peak in the bias and rms of the salinity innovations is seen in the FOAM-NEMOVAR results. The salinity increment results entirely from the unbalanced salinity. Generally speaking it is hard to argue that the altimeter data has usable information about the unbalanced salinity and therefore there is a problem with the existing scheme. To attempt to resolve this we have made a change to the vertical parametrisation of the salinity background error. The existing scheme calculates the maximum $|dS/dT|$. This value is obtained by dividing the vertical gradient of salinity (dS/dz) by the vertical gradient of temperature (dT/dz). This maximum value can easily be very deep, for example if both dS/dz and dT/dz are very small but dT/dz is close to zero. In order to constrain the depth of the maximum the scheme sets an arbitrary cap on the depth at 200 m. An East-West section at 39.55S (Fig. 9.2) shows we have very deep $|dS/dT|$ in our problem area. The value of the unbalanced salinity background error is set to the surface value above the maximum dS/dT, below this it tails off to a deep ocean value using a tanh function. In this particular region this unfortunately allows for large salinity background errors below the mixed layer (since the mixed layer lies above 200m) and consequently large unbalanced salinity increments when altimeter data is assimilated.

The solution is a new scheme which uses the mixed layer depth to determine where the unbalanced salinity background errors start to switch from the surface value to the subsurface value (set at 0.01 psu). The vertical lengthscale used in the tanh function is 100 m. The fields are also vertically and horizontally smoothed using the background covariance horizontal and vertical lengthscales.

An additional change tested was an option used by Magdalena Balmaseda at ECMWF. This option only uses the T and balanced S within the density and hence SSH balance (nfilrn2 = 4). A three month ORCA025L75 test run was performed with this fix. The results were generally good, however small scale noise was found in the equatorial regions with this particular change. Therefore, in future runs we have chosen to implement only the change to salinity background error described above. Exploring the different nfilrn2 options would be fruitful possibility for future work.

9.3 Sensitivity to bad salinity profiles

The FOAM-NEMOVAR system has occasionally shown sensitivity to poor in-situ salinity observations. The plots in Figure 30 show the SSH response to poor salinity data from one Argo float.

© Crown Copyright 2013

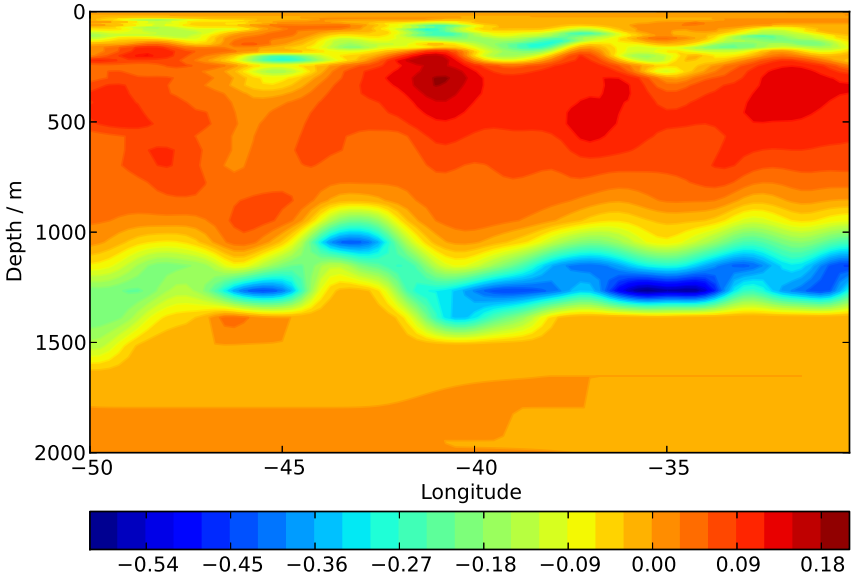

Figure 29: dS/dT E-W section at 39.55S.

The top plot in Figure 30 shows a time series of the SSH increments at (102.5W,1.75S). There is a large peak in the SSH increments every 10 days, which corresponds to the sampling period of the Argo float. The bottom plot in Figure 30 shows a field of SSH increments on a day when a poor salinity Argo observation is present. A large, spurious SSH increment can be seen in the Eastern Tropical Pacific where the bad Argo observation is located. In all cases where there was similar sensitivity to profile observation, these observations were found to be grey listed in the EN3 data set. Therefore the EN3 data set will be used in any future hindcasts to avoid this problem. However,

© Crown Copyright 2013

in order to avoid spurious results in the operational system, the quality control procedures will need to be improved to prevent these bad salinity observations from being assimilated. For instance, we could implement a quality control method based on Guinehut et al. [2009].

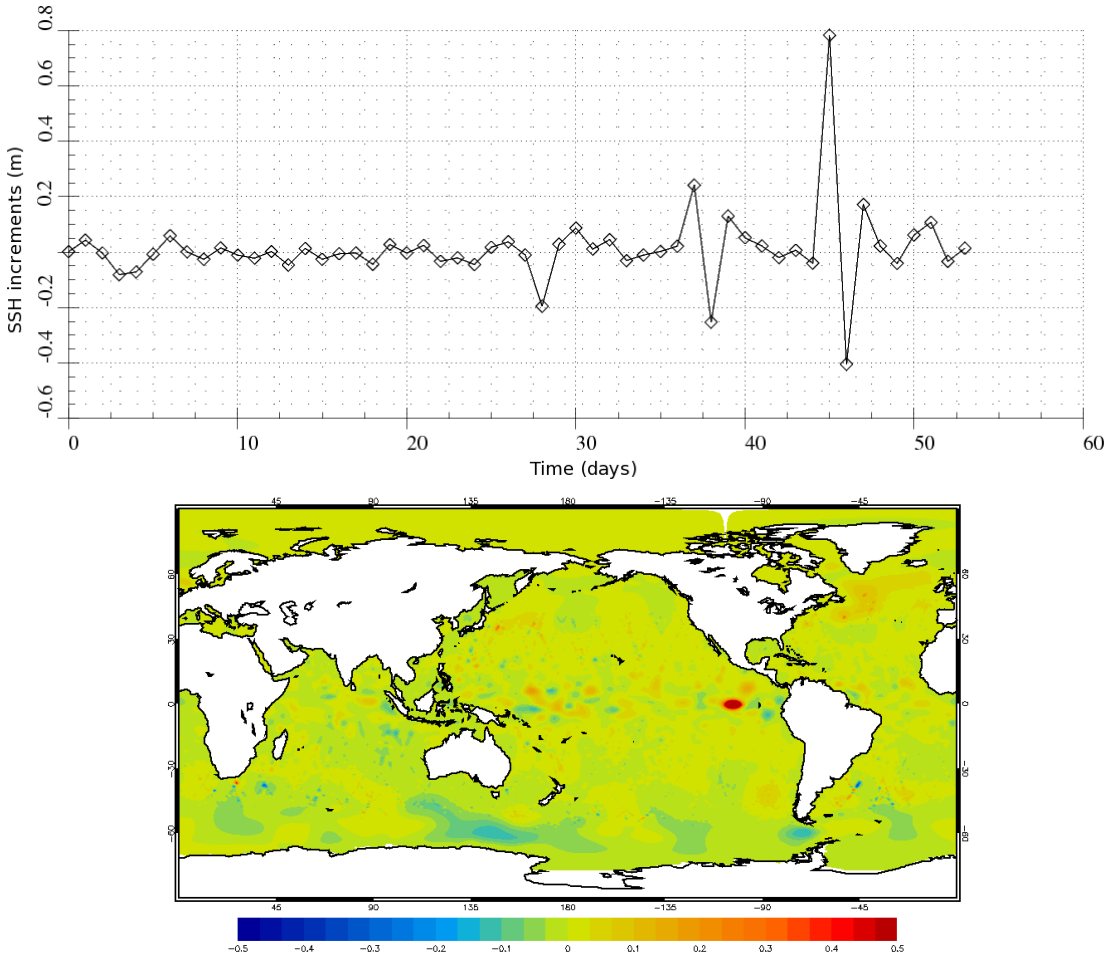

Figure 30: Plots of SSH increments. The top plot shows a time series of SSH increments at 102.5W, 1.75S starting on the 01/01/2010. The bottom plot shows a field of SSH increments on 17/02/2010.

10 Conclusions and Future work

This document describes the implementation of a new incremental 3D-VAR data assimilation system, NEMOVAR, in the Met Office's operational global $1/4$ degree model. We have given an overview of NEMOVAR and described the changes implemented at the Met Office. These include changes to the balance relationships, inclusion of sea ice concentration data assimilation, implementation of bias correction schemes for SST and altimeter and developments to the background error covariance specification. The developments to the background errors have formed a large part of this work. The temperature and salinity background error standard deviations are defined as a combination of statistical errors and parameterisations of the background fields. This allows for

© Crown Copyright 2013

flow dependent errors while substituting additional information from the statistical errors. The horizontal background error correlation lengthscales are parameterised using the Rossby radius and a new mixed layer depth dependent parameterisation is used to define the vertical lengthscales. The vertical correlation length scales are flow dependent and thus require new normalisation factors to be determined at each analysis step. An efficient method for determining the normalisation factors has been implemented. This technique uses a look-up table to generate the normalisation factors which are then used at each analysis step.
The FOAM-NEMOVAR system is compared to the preceding FOAM-AC system. The key difference between the two systems is the data assimilation method, although there are other differences which are described in Table 2. FOAM-NEMOVAR is shown to produce good improvements to surface fields with a significant improvement to SST and sea ice RMSE. There is some degradation to profile results and this will be the focus of future work with NEMOVAR. The future of the FOAM system lies in a coupled atmosphere-ocean model. Improvements to the surface field are viewed as more important in the context of couple modelling which makes FOAM-NEMOVAR the preferable system.

There have been successes and improvements seen in the new system, but there are still some areas which we wish to develop and investigate further, these are listed here-

1. Improvements to the velocities in the tropics. This should include work which focuses on the second order velocity balance.
2. More general improvements to temperature and salinity in the tropics
3. Implementation of 2 horizontal correlation lengthscales in NEMOVAR
4. Longer horizontal correlation lengthscales at depth to optimise the use of sparse deep ocean observations
5. Implementation of a T and S bias correction scheme
6. Improvement of the altimeter assimilation (in particular the SSH balance)
7. Implementation of sea ice balance
8. More controlled trials for clearer comparisons between FOAM-AC and FOAM-NEMOVAR

References

E. W. Blockley, M. J. Martin, and P. Hyder. Validation of foam near-surface ocean current forecasts using lagrangian drifting buoys. *Ocean Sci.*, 8:551–565, 2012.

S.C. Bloom, L.L. Takacs, A. M. da Silva, and D. Ledvina. Data assimilation using incremental analysis updates. *Mon. Wea. Rev*, 124:1256–1271, 1996.

© Crown Copyright 2013

J. A. Cummings. Review of the nrl multivariate ocean data assimilation system. In *7th HYCOM Consortium Meeting*, 2003.

J. A. Cummings. Operational multivariate ocean data assimilation. *Quarterly Journal of the Royal Meteorological Society*, 133:3583–3604, 2005.

N. Daget, A. T. Weaver, and M. A. Balmaseda. Ensemble estimation of background-error variances in a three-dimensional variational data assimilation system for the global ocean. *Quarterly Journal of the Royal Meteorological Society*, 135:1071–1094, 2009.

S. Dobricic and N. Pinardi. An oceanographic three-dimensional variational data assimilation scheme. *Ocean Modelling*, 22:89–105, 2008.

C. J. Donlon, M. Martin, J. D. Stark, J. Roberts-Jones, E. Fiedler, and W. Wimmer. The operational sea surface temperature and sea ice analysis (ostia). *Remote Sensing of the Environment*, 2011.

W. J. Emery, Y. Yu, G. A. Wick, P. Schluessel, and R. W. Reynolds. Correcting infrared satellite estimates of sea surface temperature for atmospheric water vapor attenuation. *Journal of Geophysical Research*, 99:5219–5236, 1994.

M. Fisher. Minimization algorithms for variational data assimilation. In *ECMWF Seminar on Recent Developments in Numerical Methods for Atmospheric Modelling*, pages 364–385, 1998.

S. Guinehut, C. Coatanoan, A.-L. Dhomps, P.-Y. Le Traon, and G. Larnicol. On the use of satellite altimeter data in argo quality control. *Journal of Atmospheric Oceanic Technology*, 26:395–402, 2009.

A. Hollingsworth and P. Lonnberg. The statistical structure of short-range forecast errors as determined from radiosonde data. part i: The wind field. *Tellus*, 38A:111–136, 1986.

E. C Hunke and W. H. Lipscomb. CICE: the Los Alamos Sea Ice Model Documentation and Software User's Manual Version 4.1. Technical report, Fluid Dynamics Group, Los Alamos National Laboratory, 2010.

A.B. Kara, P. A. Rochford, and H. E. Hurlburt. An optimal definition for ocean mixed layer depth. *Geophys. Res.*, 105(C7):16803–16821, 2000.

D. J. Lea, J. P. Drecourt, A. K. Haines, and M. J. Martin. Ocean altimeter assimilation with observational and model-bias correction. *Quarterly Journal of the Royal Meteorological Society*, 134: 1761–1774, 2008.

G. Madec. Nemo ocean engine. In *Note du Ple de modlisation*, number 27, 2003.

M. J. Martin, A. Hines, and M. J. Bell. Data assimilation in the foam operational short-range ocean forecasting system: a description of the scheme and its impact. *Quarterly Journal of the Royal Meteorological Society*, 133:981–995, 2007.

© Crown Copyright 2013

I. Mirouze and A. T. Weaver. Representation of correlation functions in variational assimilation using an implicit diffusion operator. *Quarterly Journal of the Royal Meteorological Society*, 136:1421–1443, 2010.

K. S. Mogensen. Nemovar:a variational data assimilation system for the nemo ocean model. *ECMWF Newsletter*, 120:17–21, 2009.

K. S. Mogensen, M. A. Balmaseda, and A. Weaver. The nemovar ocean data assimilation system as implemented in the ecmwf ocean analysis for system 4. Technical Report 668, ECMWF, 2012.

D. Parrish and J.C. Derber. The national meteorological center's spectral statistical interpolation analysis system. *Mon. Wea. Rev.*, 120:1747–1763, 1992.

S. Polavarapu, S. Ren, Y. Rochon, D. Sankey, N. EK, J. Koshyk, and D. Tarasick. Data assimilation with the canadian middle atmosphere model. *Atmos–Ocean*, 43:77–100, 2005.

R. J. Purser, W. Wu, D. F. Parrish, and N. M. Roberts. Numerical aspects of the application of recursive filters to variational statistical analysis. part i: Spatially homogeneous and isotropic gaussian covariances. *Mon. Wea. Rev.*, 131:1524–1535, 2003.

R. W. Reynolds, D. B. Chelton, J. Roberts-Jones, M. J. Martin, D. Menemenlis, and C. J. Merchant. Objective determination of feature resolution in two SST analyses. *Journal of Climate*, 2013.

M. H. Rio, S. Guinehut, and G. Larnicol. New CNES-CLS09 global mean dynamic topography computed from the combination of GRACE data, altimetry, and in situ measurements. *Geophys. Res.*, 116(C07018), 2011.

J. D. Stark, C. J. Donlon, M. Martin, and M. McCulloch. OSTIA : An operational, high resolution, real time, global sea surface temperature analysis system. In *OCEANS 2007 -Europe*, 2007.

A. Troccoli and K. Haines. Use of temperature-salinity relation in a data assimilation context. *Journal of Atmospheric Oceanic Technology*, 16:2011–2025, 1999.

A. T. Weaver and P. Courtier. Correlation modelling on the sphere using a generalized diffusion equation. *Quarterly Journal of the Royal Meteorological Society*, 127:1815–1846, 2001.

A. T. Weaver, J. Vialard, and D.L.T Anderson. Three- and four-dimensional variational assimilation with a general circulation model of the tropical pacific ocean. part i: Formulation, internal diagnostics, and consistency checks. *Monthly Weather Review*, 131:1360–1378, 2003.

A. T. Weaver, C. Deltel, E. Machu, S. Ricci, and N. Daget. A multivariate balance operator for variational ocean data assimilation. *Quarterly Journal of the Royal Meteorological Society*, 131: 3605–3625, 2005.

© Crown Copyright 2013

Met Office
FitzRoy Road, Exeter
Devon, EX1 3PB
UK

Tel: 0870 900 0100
Fax: 0870 900 5050
enquiries@metoffice.gov.uk
www.metoffice.gov.uk

Produced with the Met Office LaTeX template v2.0.0